USP30 sets a trigger threshold for PINK1-PARKIN amplification of mitochondrial ubiquitylation.

Emma Rusilowicz-Jones[1#], Jane Jardine[1#], Andreas Kallinos[1], Adan Pinto-Fernandez[2], Franziska Guenther[3], Mariacarmela Giurrandino[3], Francesco G. Barone[1], Katy McCarron[1], Christopher J. Burke[4,11], Alejandro Murad[4,12], Aitor Martinez[1], Elena Marcassa[1], Malte Gersch[5,6], Alex Buckmelter[4,14], Katherine J. Kayser-Bricker[4,13], Frederic Lamoliatte[10], Akshada Gajbhiye[10], Simon Davis[2], Hannah C. Scott[2], Emma Murphy[3], Katherine England[3], Heather Mortiboys[7], David Komander[8,9], Matthias Trost[10], Benedikt M. Kessler[2], Stephanos Ioannidis[4,15], Michael Ahlijanian[4,16], Sylvie Urbé[1*], Michael J. Clague[1*].

[1]Dept. of Cellular and Molecular Physiology, Institute of Translational Medicine, University of Liverpool, Liverpool, L69 3BX, UK, [2]Target Discovery Institute, Nuffield Department of Medicine, University of Oxford, Roosevelt Drive, Oxford OX3 7FZ, UK, [3] Oxford Drug Discovery Institute, Target Discovery Institute, Nuffield Department of Medicine, University of Oxford, Roosevelt Drive, Oxford OX3 7FZ, UK [4]FORMA Therapeutics, Arsenal Street, Watertown, Massachusetts 02472, USA, [5]Chemical Genomics Centre, Max-Planck-Institute of Molecular Physiology, Otto-Hahn-Str. 11, 44227 Dortmund, Germany, Technische Universität Dortmund, [6]Department of Chemistry and Chemical Biology, Otto-Hahn-Str. 4a, 44227 Dortmund, Germany, [7]Sheffield Institute for Translational Neuroscience (SITraN), University of Sheffield, 385a Glossop Road, Sheffield, S10 2HQ, UK, [8]Ubiquitin Signalling Division, The Walter and Eliza Hall Institute of Medical Research, 1G Royal Parade, Parkville, VIC 3052, Australia, [9]Department of Medical Biology, The University of Melbourne, Melbourne, VIC 3010, Australia, [10]Laboratory for Biological Mass Spectrometry, Newcastle University Biosciences Institute, Faculty of Medical Sciences, University of Newcastle, Framlington Place, Newcastle, NE2 4HH, UK.

Current addresses
[11]Yumanity Therapeutics - Discovery Biology, 790 Memorial Drive, Suite 2C, Cambridge, MA 02139 USA [12]Skyhawk Therapeutics, Neurobiology 35 Gatehouse Drive Waltham, MA 02451 USA [13]Halda Therapeutics, 23 Business Park Dr, Branford, Connecticut. USA [14]Morphic Therapeutic, 35 Gatehouse Park, Waltham, MA, USA [15]H3 Biomedicine, 300 Technology Square, Cambridge, MA 02139, USA [16]Pinteon Therapeutics, 1155 Centre Street, Newton, MA, USA.

* corresponding authors urbe@liv.ac.uk, clague@liv.ac.uk

# These authors contributed equally to this work

Running title: USP30 sets a mitophagy trigger

Key words: Parkinson’s disease, mitophagy, deubiquitylase, DUB inhibitor, ubiquitin, ubiquitylome

Summary blurb

A new inhibitor of the deubiquitylase USP30, an actionable target relevant to Parkinson's Disease, is introduced and characterised for parameters related to mitophagy.

Abstract

The mitochondrial deubiquitylase USP30 negatively regulates the selective autophagy of damaged mitochondria. We present the characterisation of a N-cyano pyrrolidine compound, FT3967385, with high selectivity for USP30. We demonstrate that ubiquitylation of TOM20, a component of the outer mitochondrial membrane import machinery, represents a robust biomarker for both USP30 loss and inhibition. A proteomics analysis, on a SHSY5Y neuroblastoma cell line model, directly compares the effects of genetic loss of USP30 with chemical inhibition. We have thereby identified a subset of ubiquitylation events consequent to mitochondrial depolarisation that are USP30 sensitive. Within responsive elements of the ubiquitylome, several components of the outer mitochondrial membrane transport (TOM) complex are prominent. Thus, our data support a model whereby USP30 can regulate the availability of ubiquitin at the specific site of mitochondrial PINK1 accumulation following membrane depolarisation. USP30 deubiquitylation of TOM complex components dampens the trigger for the Parkin-dependent amplification of mitochondrial ubiquitylation leading to mitophagy. Accordingly, PINK1 generation of phospho-Ser65 Ubiquitin proceeds more rapidly in cells either lacking USP30 or subject to USP30 inhibition.

Introduction

Damaged mitochondria are removed from the cell by a process of selective autophagy termed mitophagy. Defects in mitochondrial turnover have been linked to a number of neurodegenerative conditions including Parkinson's Disease (PD), Alzheimer's Disease (AD) and Motor Neuron Disease (MND) (Fritsch et al., 2019; Sorrentino et al., 2017). This process is best understood in the context of PD, for which loss of function mutations in the mitophagy promoting genes *PINK1* and *PRKN* (coding for the Parkin protein) are evident (Bingol and Sheng, 2016; Pickrell and Youle, 2015). Mitochondrial depolarisation leads to the accumulation of the PINK1 kinase at the mitochondrial surface, which then phosphorylates available ubiquitin moieties at Ser65 (Kane et al., 2014; Kazlauskaite et al., 2014b; Koyano et al., 2014; Ordureau et al., 2014; Wauer et al., 2015b). PhosphoSer65-Ubiquitin (pUb) recruits the ubiquitin E3 ligase Parkin to mitochondria, where it is fully activated by direct PINK1-dependent phosphorylation at Ser65 of its ubiquitin-like (UBL) domain (Gladkova et al., 2018; Jin and Youle, 2013; Kazlauskaite et al., 2014a; Wauer et al., 2015a). This triggers a feed-forward mechanism that coats mitochondria with ubiquitin, leading to selective engulfment by autophagosomal membranes (Harper et al., 2018; Pickles et al., 2018).

The deubiquitylase (DUB) family of enzymes plays a role in most ubiquitin dependent processes, by promoting ubiquitin flux or suppressing ubiquitylation of specific substrates (Clague et al., 2013; Clague et al., 2019). USP30 is one of only two DUBs that possess a trans-membrane domain. Its localisation is restricted to the outer mitochondrial membrane (OMM) and to peroxisomes (Marcassa et al., 2018; Nakamura and Hirose, 2008; Riccio et al., 2019; Urbe et al., 2012). USP30 can limit the Parkin-dependent ubiquitylation of selected substrates and depolarisation-induced mitophagy in cell systems that have been engineered to over-express Parkin (Bingol et al., 2014; Cunningham et al., 2015; Hoshino et al., 2019; Liang et al., 2015). We have recently shown that it can also suppress a PINK1-dependent component of basal mitophagy, even in cells that do not express Parkin (Marcassa et al., 2018). Thus USP30 may represent an actionable drug target relevant to PD progression and other pathologies to which defective mitophagy can contribute (Bravo-San Pedro et al., 2017; Miller and Muqit, 2019; Tsubouchi et al., 2018). One attractive feature of USP30 as a drug target in this context, is that its loss is well tolerated across a wide range of cell lines (Meyers et al., 2017).

The Ubiquitin Specific Protease (USPs) DUB family are cysteine proteases and comprise around 60 members in humans (Clague et al., 2019). Early academic efforts to obtain specific small molecule inhibitors were only partially successful (Ritorto et al., 2014). More recently industry-led efforts have generated some highly specific inhibitors, exemplified by compounds targeting USP7, an enzyme linked to the p53/MDM2 signaling axis (Gavory et al., 2018; Kategaya et al., 2017; Lamberto et al., 2017; Schauer et al., 2019; Turnbull et al., 2017). Some N-cyano pyrrolidines, which resemble known cathepsin C covalent inhibitors, have been reported in the patent literature to be dual inhibitors of UCHL1 and USP30 (Laine et al., 2011). High-throughput screening has also identified a racemic phenylalanine derivative as a USP30 inhibitor (Kluge et al., 2018). However the specificity and biological activity of this compound has so far been only characterised superficially.

Here we introduce FT3967385 (hereafter FT385), a modified N-cyano pyrrolidine tool compound USP30 inhibitor. We carefully correlate its effects upon the proteome and ubiquitylome of neuroblastoma SH5YSY cells, expressing endogenous Parkin. We also show that this compound can recapitulate effects of USP30 deletion on mitophagy and regulate the ubiquitylation status of Translocase of the Outer Mitochondrial Membrane (TOM) complex components. The TOM complex functions as a common entry portal for mitochondrial precursor proteins (Wiedemann and Pfanner, 2017). We propose that associated ubiquitin may provide nucleating sites at which PINK1 phosphorylation sets in train a feed-forward loop of further Parkin-mediated ubiquitylation (Marcassa et al., 2018). Accordingly, pUb generation following mitochondrial depolarisation is enhanced by both USP30 deletion and by inhibitor treatment.

Results

We developed a tool compound inhibitor (FT385) for investigation of USP30 biology (Figure 1A). It shows a calculated IC_{50} of ~1 nM *in vitro* using purified USP30, together with ubiquitin-rhodamine as a fluorogenic substrate (Figure 1B,E). Bio-layer interferometry experiments show binding behaviour that is consistent with covalent modification of USP30 (Figure 1C) as indicated by other studies of cyano pyrrolidine inhibitors of USPs (Bashore et al., 2020). Progress curves for Ubiquitin-rhodamine processing by USP30 were used to determine K_I *and* k_{inact} (Figure 1D,E). To test for selectivity of the inhibitor within the USP family of enzymes, we used the Ubiquigent DUB profiler screen, which tests inhibitory activity against a broad panel of USP enzymes. At the indicated concentrations (up to 200 nM) the inhibitor was highly selective for USP30 (Figure 1F). Only one other family member, the plasma membrane associated USP6, showed a significant degree of inhibition (Urbe et al., 2012). This particular deubiquitylase shows a highly restricted expression profile (Barretina et al., 2012). It is not found in any of our deep proteome data-sets, nor was it identified in two recent studies that used state of the art enrichment with active site probes to generate an inventory of cellular DUBs (Hewings et al., 2018; Pinto-Fernandez et al., 2019).

We used the competition between FT385 and Ub-propargylamide (Ub-PA), which covalently binds to the USP30 active site, to assess target engagement (Ekkebus et al., 2014). Binding of the probe to a DUB leads to an up-shift in apparent molecular weight on SDS-PAGE gels (Figure 2). If a drug is present that occupies or otherwise occludes this site, probe modification is inhibited and the protein mass is down-shifted accordingly. Our results demonstrate target engagement and allow us to determine a suitable concentration range for further experiments (Figure 2). In SHSY5Y neuroblastoma cells, effective competition of drug towards added probe is seen at concentrations >100 nM when added to cell lysates (Figure 2A) or pre-incubated with cells prior to lysis (Figure 2B).

To be able to compare compound activity to USP30 loss, we used CRISPR/Cas9 to generate YFP-Parkin-RPE1 (retinal pigment epithelium) and SH5Y5Y (neuroblastoma) USP30 knock-out (KO) cells (Figure S1). We have previously shown that USP30 physically interacts with TOM20, a component of the outer mitochondrial membrane transport complex that recognises mitochondrial targeting sequences (Liang et al., 2015; Wiedemann and Pfanner, 2017). USP30 represses both depolarisation induced mitophagy and the specific ubiquitylation of TOM20 in cells over-expressing Parkin (Bingol et al., 2014; Cunningham et al., 2015; Gersch et al., 2017; Liang et al., 2015). Application of FT385 to RPE1 cells over-expressing YFP-Parkin results in enhanced ubiquitylation and apparent loss of TOM20 without affecting PINK1 protein levels (Figure 3A). Enhancement of TOM20 ubiquitylation by FT385 under depolarising conditions is more clearly shown in Figure 3B. In this experiment, a shorter depolarisation time (1 hour) has been used, at which there is minimal TOM20 loss to mitophagy or other pathways. USP30 KO and inhibitor treated cells show similar elevation of ubiquitylated TOM20, whilst no further enhancement is achieved by inhibitor treatment of KO cells (Figure 3B). Thus, the TOM20 ubiquitylation response depends on USP30 catalytic activity and represents an on-target effect of the drug.

We confirmed that both USP30 deletion and inhibition can also lead to the accumulation of ubiquitylated TOM20 in SHSY5Y cells, both in whole cell lysates and in crude mitochondrial fractions (Figure 3C,D and Figure S2A-F). Here, we are detecting this modification without Parkin over-expression. TOM20 is atypical in the respect that we do not observe USP30-dependent changes to the ubiquitylation pattern of another mitochondrial Parkin substrate Mitofusin 2 (MFN2) (Figure 3A,C,D and Figure S2A). To determine effects of USP30 inhibition on basal mitophagy, we used SHSY5Y cells expressing a tandem mCherry–GFP tag attached to the outer mitochondrial membrane localization signal of the protein FIS1 (mitoQC) (Allen et al., 2013). A clear increase in the number of mitolysosomes per cell, indicative of increased mitophagic flux, is apparent following USP30 inhibition over a 96 hour time period (Figure 3E).

Trypsin digestion of ubiquitylated proteins generates peptides with a residual diGly motif, which provides a characteristic mass shift and can be used for enrichment by immunoprecipitation (Peng et al., 2003). Several studies have used this approach to define Parkin substrates through proteomic analysis, following mitochondrial depolarisation in cell lines over-expressing Parkin (Ordureau et al., 2018; Ordureau et al., 2014; Sarraf et al., 2013). In order to search for potential substrates and/or biomarkers beyond TOM20, we decided to take an unbiased view of USP30 control of the cellular proteome and ubiquitylome in SHSY5Y cells, which endogenously express Parkin. Our experimental design, using triplexed combinations of SILAC labels, allowed quantitative comparison of both USP30 inhibitor treated (200 nM) and USP30 KO relative to parental untreated cells in basal conditions (proteome) or following mitochondrial depolarisation (proteome + ubiquitylome) (Figure 4A). We quantitated 6,423 proteins and 9,536 diGly peptides (which indicate specific sites of ubiquitylation), derived from 2,915 proteins (Table S1). We had hoped that the proteome might provide a biomarker that could be used in pre-clinical models for testing drug efficacy. Despite obtaining deep proteome coverage, we identified few proteins that responded to both genetic deletion and inhibition of USP30 (24 hours) in a consistent manner across experiments. No impact of USP30 on total mitochondrial or peroxisomal mass following 24 hours depolarisation is apparent (Figure 4B). This is in keeping with our observations and previous findings, that in cell lines expressing endogenous levels of Parkin, the extent of depolarisation-induced mitophagy is low (Rakovic et al., 2013). In this experiment we find that USP30 influences the ubiquitylation status of a small minority of proteins following depolarisation (Figure 4C). Most prominent among them are members of the voltage dependent anion channel (VDAC) family. VDAC1, VDAC2 and VDAC3 show enhanced ubiquitylation at specific sites in the absence of USP30 activity without any change at the proteome level. In general, the effect is stronger in the USP30 KO cells but the pattern is conserved with USP30 inhibitor treatment (Figure 4C-E, Figure S3A B). Some proteins show a response to inhibitor but not to genetic loss of USP30 (for details see Table S1 and Figure S3C). There is no obvious connection between these proteins or enrichment for mitochondrial annotation and they likely represent off-target effects. One conclusion from these data is that the global impact of USP30 activity at both the proteome and ubiquitylome levels is subtle. This makes pharmacology in both terminally differentiated cellular models (e.g., primary cultured rodent neurons or human iPSC-derived neurons) and *in vivo* experiments challenging. However, it is consistent with low impact on cell viability seen in CRISPR screens (Hart et al., 2017) and may in fact be a desirable feature of a drug target for a neurodegenerative disease.

To obtain information on the early USP30-dependent changes to the mitochondrial ubiquitylation profile that follow depolarisation, we compared two USP30 KO SHSY5Y clones with wild type cells, using a shorter depolarisation period (4 hours, Figure 5A). No systematic changes in mitochondrial or peroxisomal protein abundance were observed (Figure 5B). For the ubiquitylome arm of this experiment we used crude mitochondrial fractions to increase coverage of specific mitochondrial components. This is evident in Figures 5C and 5D, which summarise the major changes in ubiquitylation we have identified at specific sites in both sets of experiments (Figures 4A and 5A, Figure S3D,E, Tables S1 and S2). Multiple responsive VDAC peptides were once again identified. Strong outliers are found in Ganglioside-induced differentiation associated protein 1 (GDAP1), an outer mitochondrial membrane protein, mutations of which are linked to Charcot-Marie-Tooth neuropathy and mitochondrial dysfunction (Barneo-Munoz et al., 2015) and the mitochondrial outer membrane protein Synaptojanin 2 binding protein (SYNJ2BP, Figure 5D and E) (Nemoto and De Camilli, 1999). Also prominent is Peptidyl-tRNA Hydrolase 2 (PTRH2), a mitochondrial protein linked to the release of non-ubiquitylated nascent chains from stalled ribosomal complexes (Kuroha et al., 2018). The improved coverage now also reveals USP30-dependent ubiquitylation of multiple TOM complex components including the two translocase receptors, TOM20 and TOM70, the TOM40 channel and an accessory subunit TOM5 within this set of strong outliers.

In healthy mitochondria, PINK1 is imported through the TOM complex and subsequently cleaved and released for proteasomal degradation in the cytosol. In depolarised mitochondria it is no longer imported and degraded but remains associated with TOM complex components on the outer mitochondrial membrane (Lazarou et al., 2012; Okatsu et al., 2015; Okatsu et al., 2013; Sekine and Youle, 2018). At this point it becomes trans-activated and initiates a signaling cascade by phosphorylating ubiquitin on Ser65 (generating pUb). This accumulation of pUb can be readily visualised by Western blotting using a specific antibody. We find that genetic loss of USP30 or USP30 inhibition both lead to a more rapid accumulation of pUb following mitochondrial depolarisation, without an evident increase in total PINK1 nor Parkin levels at mitochondria (Figures 6A-D and Figure S4).

Discussion

Here we provide a comprehensive analysis of the impact of USP30 on mitochondrial ubiquitylation dynamics following mitochondrial membrane depolarisation. Our principal analysis is conducted on cells expressing endogenous levels of Parkin and we directly compare the effects of genetic loss with a specific inhibitor. This allows us to clearly attribute molecular signatures to catalytic activity for the first time. We have extended USP30 linkage to the mitochondrial import (TOM) complex to now include subunits beyond TOM20, which has been previously characterised (Bingol and Sheng, 2016; Gersch et al., 2017; Liang et al., 2015). We also identify a further substrate, SYNJ2BP, whose enhanced ubiquitylation can be monitored by Western blotting. Based on our studies FT385 emerges as a promising tool compound for the study of USP30 biology. When used at appropriate concentrations, a high degree of specificity amongst DUB family members can be achieved. On the other hand, there are some inevitable liabilities; following inhibitor treatment, we identified several proteins with enhanced ubiquitylation that are not evident with genetic loss of USP30.

Previous studies have suggested that the overall pattern of depolarisation-induced ubiquitylation of mitochondria is largely unchanged following USP30 knock-down, with TOM20 being an exception (Gersch et al., 2017; Liang et al., 2015). We see enhanced pUb accumulation in the absence of USP30 activity, despite the published observations that pUb modified chains provide a poor substrate for USP30 (Gersch et al., 2017; Wauer et al., 2015b). How then might USP30 suppress mitophagy, as previously reported in several studies (Bingol et al., 2014; Cunningham et al., 2015; Liang et al., 2015; Marcassa et al., 2018)? We have previously shown that USP30 depletion enhances PINK1-dependent basal mitophagy even in the absence of Parkin (Marcassa et al., 2018). We and others have proposed that USP30 may regulate the availability of ubiquitin on specific trigger proteins that are most readily available for phosphorylation by PINK1. In other words, USP30 may determine the probability that a local accumulation of PINK1 can trigger feed-forward mechanisms that lead to mitophagy (Clague and Urbe, 2017; Gersch et al., 2017; Marcassa et al., 2018). The prominence of TOM complex components within the limited set of USP30-responsive diGly-peptides, and the known interaction with both USP30 (Liang et al., 2015) and with PINK1 (Lazarou et al., 2012; Okatsu et al., 2015; Okatsu et al., 2013; Sekine and Youle, 2018) suggest that this may be a critical pUb nucleation site regulated by USP30 (Figure 7).

Whilst our manuscript was in preparation, two complementary studies have been published that also highlight the centrality of the TOM complex to USP30 function (Ordureau et al., 2020; Phu et al., 2020). All three studies use global proteome and ubiquitylome profiling. Ordureau et al. examine the impact of USP30 genetic loss in iNeurons ± AO (Ordureau et al., 2020). Phu et al. focus on basal conditions (no depolarisation agents) and use HEK293 cells to compare genetic loss with a USP30 inhibitor that is related to the one we describe here (Phu et al., 2020). Note that, in that latter study a much higher concentration of inhibitor has been used (5 µM vs 200 nM). We identify an overlapping set of USP30-sensitive ubiquitylation sites with these studies. Our findings are more directly comparable with Ordureau et al., as our data derive from AO-treated cells. For the majority (15/16) of USP30-sensitive mitochondrial proteins we describe in our ubiquitylome analysis (Figure 5C), corresponding increases have also been found in USP30 KO iNeurons, albeit the specific sites differ in some instances (Ordureau et al., 2020). Both studies find greater prevalence, than we do here, of elevated ubiquitylation of mitochondrial matrix and inner mitochondrial membrane proteins, although we do see a few examples of the same phenomenon (e.g. MDH2, GRSF1, MTLN). Although ubiquitylation can occur within mitochondria (Lavie et al., 2018), USP30 is an outer mitochondrial membrane protein whose catalytic activity is facing towards the cytosol (Marcassa et al., 2018; Nakamura and Hirose, 2008). Hence, it has been suggested that this reflects ubiquitylation of newly synthesised proteins engaging with the TOM complex (Ordureau et al., 2020; Phu et al., 2020). Thus USP30 might sit at the gate of the import complex pore and strip off ubiquitin as a prerequisite for entry. This provides a striking parallel with the action of proteasomal deubiquitylases, which control entry to the proteasome core (Lee et al., 2011). Ribosomes themselves interact directly with the TOM complex (Gold et al., 2017) and ribosomal quality control (RQC) mechanisms have extensive links to the ubiquitin system (Joazeiro, 2017). Perturbation of these pathways, could also lead to a higher representation of ubiquitylated peptides derived from nascent imported proteins. Our finding that the mitochondrial peptidyl-tRNA hydrolase PTRH2 is a USP30 substrate provides a first link to RQC. PTRH2 can cleave nascent chain tRNA on stalled ribosomes and provide a release mechanism for non-ubiquitylated nascent chains (Kuroha et al., 2018).

The USP30 dependent suppression of mitophagy is well established for events which rely on the over-expression of Parkin, together with acute mitochondrial depolarisation (Bingol et al., 2014; Cunningham et al., 2015; Liang et al., 2015). In fact, in a recently published whole genome screen for mitophagy regulators in Parkin overexpressing C2C12 myoblasts, USP30 is the most prominent mitochondrial annotated negative regulator (Hoshino et al., 2019). Our study contributes to a body of evidence that translates these finding to systems with endogenous Parkin expression levels (Marcassa et al., 2018; Ordureau et al., 2020; Phu et al., 2020). The physiological defects associated with PINK1/Parkin loss of function in Parkinson’s Disease are likely to accumulate slowly. The benign effects of USP30 loss or inhibition, make it a target candidate that can be considered for long-term therapy. The availability of specific tool compounds, such as described here, will enable pre-clinical assessment of this strategy.

Materials and Methods

Cell culture

hTERT-RPE1-YFP-PARKIN (Liang et al., 2015), SHSY5Y and SHSY5Y-mitoQC (mCherry-GFP-Fis1(101-152)) (Allen et al., 2013) cells were routinely cultured in Dulbecco's Modified Eagle's medium DMEM/F12 supplemented with 10% FBS and 1% non-essential amino acids.

Generation of USP30 knockout cells

USP30 knockout (KO) cells were generated using CRISPR-Cas9 with USP30 specific sgRNAs targeting exon 3 of isoform 1 (sgRNA1: AGTTCACCTCCCAGTACTCC, sgRNA2: GTCTGCCTGTCCTGCTTTCA). sgRNAs were cloned into the pSpCas9(BB)-2A-GFP (PX458) vector (Addgene plasmid #48138 46) or PX330-Puro (kind gift from Prof Ciaran Morrison, NUI Galway). hTERT-RPE1-YFP-Parkin USP30 knockout Clone 1E and SHSY5Y clones KOC and KOD were engineered by transfecting the parental lines with pSpCas9(BB)-2A-GFP-sgRNA1, followed by FACS 24 hours later (selection for GFP positive cells) and single cell dilution. SHSY5Y-mitoQC Clone 11 was engineered by transfection with PX330-Puro-sgRNA2 followed by selection with 1-1.5 μg/ml Puromycin and single cell dilution. The positive clone (KO11) has lost expression of the mitoQC fluorophore. Individual clones of SHSY5Y KO cells were amplified and multiple alleles sequenced (Figure S1).

Antibodies and reagents

Antibodies and other reagents used were as follows: anti-USP30 (Sigma HPA016952, 1:500), anti-USP30 (Thermo Fisher, PA5-53523, 1:1000), anti-USP30 (MRC PPU, Dundee, 1:1000), anti-USP30 (Santa-Cruz, sc-515235, 1:1000), anti-PINK1 (Fig 1E; D8G3, Cell Signalling Technology, 6946S, 1:1000), anti-TOM20 (Sigma HPA011562, 1:1,000), anti-PARK2 (SantaCruz, sc32282, 1:250), anti-MFN2 (Abcam, ab56889, 1:1000), anti-ubiquitin (Lifesensor, VU101, 1:2000), anti-FIS1 (ProteinTech, 10956-1-AP, 1:1000), anti-phospho-Ubiquitin Ser65 (Millipore, ABS1513-I, 1:1000), anti-phosphoUbiquitin Ser65 (Cell Signalling Technology, 62802, 1:1000), anti-VDAC1 (Abcam, ab15895, 1:1000), mouse anti-actin (Abcam ab6276, 1:10,000), mouse anti-actin (ProteinTech

66009-1-Ig, 1:10,000), rabbit-anti-actin (ProteinTech,20536-1-AP, 1:10,000), anti-SYNJ2BP (Sigma HPA000866, 1:1000), oligomycin A (SIGMA 75351), antimycin A (SIGMA A8674).

Preparation cell lysates and Western blot analysis

Cultured cells were either lysed with urea buffer (Figure 6E, 9 M urea, 20 mM Hepes-NaOH pH 7.4) supplemented with 2-Chloroacetamide (CAA, Sigma) or NP-40 (0.5% NP-40, 25 mM Tris–HCl pH 7.5, 100 mM NaCl, 50 mM NaF) lysis buffer and routinely supplemented with mammalian protease inhibitor (MPI) cocktail (Sigma) and Phostop (Roche), with the exception of data presented in Figure 2. Proteins were resolved using SDS–PAGE (Invitrogen NuPage gel 4–12%), transferred to nitrocellulose membrane, blocked in 5% milk, 5% BSA or 0.1% Fish Skin Gelatin in TBS supplemented with Tween-20, and probed with primary antibodies overnight. Visualisation and quantification of Western blots were performed using IRdye 800CW and 680LT coupled secondary antibodies and an Odyssey infrared scanner (LI-COR Biosciences, Lincoln, NE).

Sub-cellular fractionation

SHSY5Y cells were washed with ice-cold PBS and then collected by scraping and centrifugation at 1000 g for 2 minutes. Cell pellets were washed with HIM buffer (200 mM mannitol, 70 mM sucrose, 1 mM EGTA, 10 mM HEPES-NaOH pH 7.4) and then resuspended in HIM buffer supplemented with mammalian protease inhibitors. Cells were mechanically disrupted by shearing through a syringe with a 27G needle, followed by passing 3 times though a 8.02 mm diameter "cell cracker" homogeniser using a 8.01 mm diameter ball bearing (Aubry and Klein, 2006) or passage through a 27G needle (Figure 2A). The resulting homogenate was cleared from nuclei and unbroken cells by centrifugation at 600 g for 10 minutes to obtain a post nuclear supernatant (PNS). The PNS was separated into the post-mitochondrial supernatant (PMS) and crude mitochondrial fraction (MF) by centrifugation at 7000 g for 15 minutes. The MF pellet was resuspended in HIM buffer + MPI.

Activity probe assay

Cells were mechanically homogenised in HIM buffer supplemented with 1 mM DTT (Figure 2A) or 1 mM Tris(2-carboxyethyl)phosphine (TCEP, Figure 2B) to obtain the PNS. Homogenates were incubated with Ub- propargyl (Ub-PA) probe at 1:100 (w/w) for 15 minutes at 37°C (Ekkebus et al., 2014). The reaction was stopped by the addition of sample buffer and heating at 95°C. To test drug engagement either intact cells or cell homogenate (PNS, without addition of protease inhibitors) were treated with FT385. Intact cells were treated for 4 hours at 37°C prior to homogenisation and homogenate was pre-incubated for 30 minutes at room temperature before probe incubation. Samples were either processed using a WES system and transformed to a virtual Western blot (Figure 2A, Protein Simple, Biotechne) or analysed by standard Western blot (Figure 2B).

SILAC Labelling

SHSY5Y and SHSY5Y-KO11 cells were grown for at least 8 passages in SILAC DMEM/F12 supplemented with 10% dialysed FBS, 200 mg/L L-proline and either L-lysine (Lys0) together with L-arginine (Arg0), L-lysine-$^{2}H_4$ (Lys4) with L-arginine-U-$^{13}C_6$ (Arg6) or L-lysine-U-$^{13}C_6$-$^{15}N_2$ (Lys8) with L-arginine-U-$^{13}C_6$-$^{15}N_4$ (Arg10) at final concentrations of 28 mg/L arginine and 146 mg/L lysine.

Proteomics methods

For the experiments shown in Figure 4, SILAC labelled cells, were lysed by sonication in 9 M urea, 20 mM HEPES pH 8.0, 1 mM sodium orthovanadate, 2.5 mM sodium pyrophosphate, 1 mM glycerol-3-phosphate. In experiments 1 and 2 the "medium" samples (Fig 4A) are derived form the same lysate. For total proteome and ubiquitylome, 700 µg and 20 mg respectively, of each sample was combined at a 1:1:1 ratio respectively. For the experiments shown in Figure 5, Mitochondrial fractions (MF, ubiquitylome) were obtained by homogenisation in HIM buffer supplemented with mammalian protease inhibitors, 50 mM CAA and Phostop from SILAC labelled cells. Cell pellets (proteome) or MFs were lysed by sonication in 9 M urea, 20 mM HEPES pH 8.0, 1.15 mM sodium molybdate, 1 mM sodium orthovanadate, 4 mM sodium tartrate dihydrate, 5 mM glycerol-3-phosphate, 1 mM sodium fluoride, then reduced and alkylated with either 4.5 mM dithiothreitol/10 mM iodoacetamide (Figure 4) or 10 mM TCEP/10 mM CAA (Figure 5). Urea was then diluted 4 fold by the addition of 20 mM HEPES buffer prior to trypsinisation overnight. The resultant tryptic peptides were acidified with Trifluoroacetic acid and purified on a C18 Sep-Pak column before lyophilisation (Figure 4) or drying with a SpeedVac (Figure 5).

For ubiquitylome samples, modified peptides were enriched by immunoprecipitation using a diGly specific antibody in accordance with manufacturer's instructions (PTMScan Ubiquitin

Remnant Motif (K-GG) Kit #5562, Cell Signaling Technology). Eluted peptides were purified using C18 stage tips (Figure 4) or C18 Sep-Pak columns (Figure 5). Samples were then dried in a speed-vac before resuspension and analysis by LC-MS/MS. Ubiquitylome (Figure 4) samples were analysed (total 5 technical replicates) on an Orbitrap Fusion Lumos (1 replicate) and Orbitrap Q Exactive HF (4 replicates). Ubiquitylome (Figure 5) samples were analysed on an Orbitrap Fusion Lumos.

For proteome samples, peptides were separated by fractionation. For Figure 4, samples were fractionated by off-line high-pH reverse-phase pre-fractionation as previously described (Davis et al., 2017), with the exception that eluted peptides were concatenated down to 10 fractions. Briefly, digested material was fractionated using the loading pump of a Dionex Ultimate 3000 HPLC with an automated fraction collector and a XBridge BEH C18 XP column (3 × 150 mm, 2.5 µm particle size, Waters no. 186006710) over a 100 minute gradient using basic pH reverse-phase buffers (A: water, pH 10 with ammonium hydroxide; B: 90% acetonitrile, pH 10 with ammonium hydroxide). The gradient consisted of a 12 minute wash with 1% B, then increasing to 35% B over 60 minutes, with a further increase to 95% B in 8 minutes, followed by a 10 minute wash at 95% B and a 10 minute re-equilibration at 1% B, all at a flow rate of 200 µl/min with fractions collected every 2 minutes throughout the run. 100 µl of the fractions was dried and resuspended in 20 µL of 2% acetonitrile/0.1% formic acid for analysis by LC–MS/MS. Fractions were loaded on the LC–MS/MS following concatenation of 50 fractions into 10, combining fractions in a 10-fraction interval (F1 + F11 + F21 + F31 + F41… to F10 + F20 + F30 + F40 + F50). For Figure 5, samples were fractionated by off-line reverse-phase pre-fractionation using a Dionex Ultimate 3000 Off-line LC system. Briefly, digested material was fractionated using the loading pump of a Dionex Ultimate 3000 HPLC with an automated fraction collector and with a Gemini C18, (3 µm particle size, 110A pore, 3 mm internal diameter, 250 mm length, Phenomenex #00G-4439-Y) over a 39 minute gradient using the following buffers: A: 20 mM Ammonium Formate, pH=8; B: 100% ACN. The gradient consisted of a 1 minute wash with 1% B, then increasing to 35.7% B over 28 minutes, followed by a 5 minute wash at 90% B and a 5 minute re-equilibration at 1% B, all at a flow rate of 250 µl/min. with fractions collected every 45 seconds from 2 minutes to 38 minutes for a total of 48 fractions. Non-consecutive concatenation of every 13th fraction was used to obtain 12 pooled fractions (Pooled Fraction 1: Fraction 1 + 13 + 25 + 27, Pooled Fraction 2 : Fraction 2 + 14 + 26 + 38 ...).

Orbitrap Q Exactive HF LC-MS/MS parameters

Peptide fractions were analysed by nano-UPLC-MS/MS using a Dionex Ultimate 3000 nano UPLC with EASY spray column (75 µm x 500 mm, 2 µm particle size, Thermo Scientific) with a 60 minute gradient of 2% acetonitrile, 0.1% formic acid in 5% DMSO to 35% acetonitrile, 0.1% formic acid in 5% DMSO at a flow rate of ~250 nl/minute. MS data was acquired with an Orbitrap Q Exactive HF instrument in which survey scans were acquired at a resolution of 60,000 at 200 m/z and the 20 most abundant precursors were selected for HCD fragmentation with a normalised collision energy of 28.

Orbitrap Fusion Lumos LC-MS/MS parameters

Samples (Figures 4 & 5) were analysed by LC-MS/MS on a Dionex Ultimate 3000 connected to an Orbitrap Fusion Lumos. For experiments presented in Figure 4 peptides were separated using a 60 minute linear gradient from 2–35 % acetonitrile in 5% DMSO, 0.1% formic acid at a flow rate of 250 nl/min. on a 50 cm EASY spray column (75 µm x 500 mm, 2 µm particle size, Thermo Scientific). For experiments presented in Figure 5 peptides were separated using 120 (proteome) or 240 (ubiquitylome) minute linear gradients from 0–28% acetonitrile in 3% DMSO, 0.1% formic acid at a flow rate of 300 nl/min. on a 50cm EASY spray column (75 µm x 500 mm, 2 µm particle size, Thermo Scientific). MS1 scans were acquired at a resolution of 120,000 between 400 – 1,500 m/z with an AGC target of $4x10^5$. Selected precursors were fragmented using HCD at a normalised collision energy of 28% (Figure 4) or 30% (Figure 5), an AGC target of $4x10^3$ (Figure 4) or $4 x10^4$ (Figure 5), a maximum injection time of 35 ms (Figure 4) or 45 ms (Figure 5), a maximum duty cycle of 1 second (Figure 4) or 3 seconds (Figure 5) and a dynamic exclusion window of 60 seconds (Figure 4) or 45 seconds (Figure 5). MS/MS spectra were acquired in the ion trap using the rapid scan mode.

Mass spectrometry data analysis

All raw MS files from the biological replicates of the SILAC-proteome experiments were processed with the MaxQuant software suite; version 1.6.7.0 using the Uniprot database (retrieved in July 2019) and the default settings (Tyanova et al., 2016). Cysteine carbamidomethylation was set as a fixed modification, whereas oxidation, phospho(STY), GlyGly (K) and acetyl N terminal were considered as variable modifications. Data was requantified. ProteinGroup text files (proteome) or GlyGly (K) sites files were further processed using Excel (see Table S1) and Perseus (version 1.6.10.50). Graphs were plotted using JMP13. Heatmaps were generated using Morpheus (Broad Institute).

In Vitro USP30 Activity Assay

Fluorescence intensity measurements were used to monitor the cleavage of a ubiquitin-rhodamine substrate. All activity assays were performed in black 384-well plates in 20 mM Tris-HCl, pH 8.0, 0.01 % Triton-X, 1 mM L-Glutathione and 0.03% Bovine Gamma Globulin with a final assay volume of 20µl. Compound IC_{50} values for DUB inhibition were determined as previously described (Turnbull et al., 2017). Briefly, an 11-point dilution series of compounds were dispensed into black 384-well plates using an Echo (Labcyte). USP30, 0.2 nM (#E-582 residues 57-517, Boston Biochem) was added and the plates pre-incubated for 30 minutes. 25 nM ubiquitin-rhodamine 110 (Ubiquigent) was added to initiate the reaction and the fluorescence intensity was recorded for 30 minutes on a Pherastar FSX (BMG Labtech) with a 485 nm excitation/520 nm emission optic module. Initial rates were plotted against compound concentration to determine IC_{50}.

k_{inact}/K_I determination

A k_{inact}/K_I assay was carried out using 0.2 nM USP30 and 180 nM ubiquitin-rhodamine 110 as described above with the omission of the 30 minute pre-incubation step. Upon addition of the substrate, fluorescence intensity was monitored kinetically over 30 minutes. Analysis was performed in GraphPad Prism. Kinetic progress curves were fitted to equation $y = (vi/k_{obs})(1 - \exp(-k_{obs}x))$ to determine the k_{obs} value. The k_{obs} value was then plotted against the inhibitor concentration and fitted to the equation $y = k_{inact}/(1 + (K_I/x))$ to determine k_{inact} and K_I values.

Bio-layer interferometry

Bio-layer interferometry was performed on an Octet RED384® system (ForteBio) at 25°C in a buffer containing 50 mM HEPES buffer (pH 7.5), 400 mM NaCl, 2 mM TCEP, 0.1% Tween, 5% Glycerol and 2% DMSO. Biotinylated USP30 (residues 64-502Δ179-216 & 288-305, Viva Biotech Ltd., Shanghai) was loaded onto Superstreptavidin (SSA) biosensors. Association of defined concentrations of FT385 (0–6.67 µM) was recorded over 180 seconds followed by dissociation in buffer over 600 seconds. Traces were normalised by double subtraction of baseline (no USP30, no compound) and reference sensors (no USP30, association and dissociation of compound) to correct for non-specific binding to the sensors. Traces were analysed using Octet Software (Version 11.2, ForteBio).

Live cell imaging and basal mitophagy quantification

SHSY5Y cells stably expressing mCherry-GFP-Fis1 (101-152) (SHSY5Y mitoQC) (Allen et al., 2013) were treated every 24 hours over a 96 hours timecourse with 200 and 500 nM of FT385. Cells were re-plated onto a IBIDI µ-Dish (2x10^5) two days before live-cell imaging with a 3i Marianas spinning disk confocal microscope (63x oil objective, NA 1.4, Photometrics Evolve EMCCD camera, Slide Book 3i v3.0). Cells were randomly selected using the GFP signal and images acquired sequentially (488 nm laser, 525/30 emission; 561nm laser, 617/73 emission). Analysis of mitophagy levels was performed using the 'mito-QC Counter' implemented in FIJI v2.0 software (ImageJ, NIH) as previously described (Montava-Garriga et al., 2020), using the following parameters: Radius for smoothing images = 1.25, Ratio threshold = 0.8, and Red channel threshold = mean + 0.5 standard deviation. Mitophagy analysis was performed for three independent experiments with 80 cells per condition. One-Way ANOVAs with Dunnett's multiple comparisons were performed using GraphPad Prism 6. *P*-values are represented as $^{**}P < 0.01$, $^{****}P < 0.0001$. Error bars denote standard deviation.

Data availability

The mass spectrometry data from this publication have been deposited to the ProteomeXchange Consortium via the PRIDE partner repository and assigned the identifier PXD019692 (Data in figure 4) and PXD018640 (Data in figure 5).

Acknowledgements

We thank Jon Lane and Ian Ganley for provision of cell lines. Funding for development of FT385 was provided by Forma Therapeutics. Additional support was provided by Celgene, Michael J. Fox Foundation, Alzheimer's Research UK (MG, EM, KE), Parkinson's UK (H-1502 JJ), MRC (MR/N00941X/1 EM, AK, KM), Wellcome Trust (FGB, AG), European Union (FL). Funding for ODDI was obtained by John Davis.

Author contributions

Conceptualisation (MJC,SU,DK,HM,BMK,MA,SI), biological investigation, chemistry and data analysis (ER-J,JJ,AK,AP-F,FG,MG,FGB,KM,CJB,AM,AM,EM,MG,AB,KJK-B,FL,AG,SD,HCS,EM,KE) Writing original draft (MJC,SU,ER-J,JJ), Writing, review and editing (MJC, SU, ER-J, JJ, AK, AP-F, MG, MT, HM, DK, BMK, KJK-B, SI, MA).

Conflict of interest

The authors declare that they have no conflict of interest.

Figure Legends

Figure 1. FT3967385 is a selective covalent USP30 inhibitor.

(A) Chemical structure of FT3967385 (FT385). (B) Concentration dependent inhibition of recombinant USP30 activity using ubiquitin-rhodamine as a substrate. (C) Bio-layer interferometry (BLI) traces showing no significant off-rate at indicated concentrations. Red line indicates removal of the inhibitor after 180 seconds. (D) Progress curves characteristic of a covalent inhibitor (0-6.67 µM), these are fitted to obtain K_I and k_{inact}. (E) Data table of inhibitory properties. (F) DUB specificity screen (DUB profiler, Ubiquigent) with 2, 20 and 200 nM FT385.

Figure 2. Activity based ubiquitin probe assay shows that FT385 engages USP30 in cells at low nanomolar concentrations. (A) SHSY5Y cell homogenates or (B) intact SHSY5Y cells were incubated with FT385 for 30 minutes or 4 hours respectively at the indicated concentrations, then incubated with Ub-PA probe for 15 minutes at 37°C and immunoblotted as shown. Samples in (A) were analysed using an automated western blot (WES™) system.

Figure 3. Pharmacological inhibition of USP30 phenocopies USP30 KO in enhancing basal mitophagy and promoting ubiquitylation of TOM20 upon depolarisation.

(A) Inhibition of USP30 enhances the ubiquitylation and degradation of TOM20 in YFP-Parkin over-expressing hTERT-RPE1 cells in response to mitophagy induction. Cells were treated for 4 hours with DMSO or Antimycin A and Oligomycin A (AO; 1 µM each) in the absence or presence of 200 nM FT385, lysed and analysed by western blotting. (B) USP30 inhibitor (FT385) treatment of parental YFP-Parkin over-expressing hTERT-RPE1 cells phenocopies USP30 deletion (KO1E) by promoting TOM20 ubiquitylation. In contrast, TOM20 ubiquitylation is unaffected by FT385 in the USP30 KO (KO1E) cells. Cells were treated for 1 hour with or without AO (1 µM) in the absence or presence of 200 nM FT385, lysed and samples analysed by immunoblotting. (C) TOM20 ubiquitylation is enhanced by USP30 inhibition and deletion in SHSY5Y cells expressing endogenous Parkin. SHSY5Y with or without FT385 (200 nM) and USP30 CRISPR/Cas9 KO cells (KO11 and KOD, two distinct sgRNAs) were treated with AO (1 µM each) for 4 hours as indicated. Cells were then lysed and samples analysed by immunoblotting as shown. Graph shows quantification of ubiquitylated TOM20 normalised to unmodified TOM20 for two independent experiments with individual data points shown in dark and light blue. Error bars indicate the range. (D) SHSY5Y (mitoQC) and USP30 KO cells (KO11) were treated for 24 hours with AO (1 µM each) in the presence or absence of FT385 (100 nM). Cells were subjected to sub-cellular fractionation and the mitochondria-enriched fraction (MF) was analysed by immunoblotting as indicated. Bar chart shows quantification of ubiquitylated TOM20 normalised to unmodified TOM20. (A-D) Black and red arrowheads indicate unmodified and ubiquitylated TOM20 or MFN2 species respectively (high exp. = higher exposure). (E) Quantification of the number of mitolysosomes in SHSY5Y-mitoQC cells, treated with DMSO or FT385 (200 or 500 nM) for 96 hours prior to imaging. Average ± SD; n=3 independent experiments; 80 cells per experiment; one-way ANOVA with Dunnett's multiple comparisons test, $^{**}P < 0.01$, $^{****}P < 0.0001$.

Figure 4. Comparison of Proteome and Ubiquitylome changes in USP30 KO versus USP30 inhibitor treated SHSY5Y cells.

(A) Schematic flow-chart of SILAC based quantitative ubiquitylome and proteome analysis comparing USP30 KO and USP30 inhibition. SHSY5Y (USP30 wild-type) and SHSHSY USP30 KO (KO11) cells were metabolically labelled by SILAC as shown. Cells were then treated for 24 hours with DMSO or Antimycin A and Oligomycin A (AO; 1 µM each) and/or FT385 (200 nM) as indicated. Cells were lysed and processed for mass spectrometry analysis.

Graphs depicting the fold change ($\log_2$) in the proteome (B) or ubiquitylome (C) of AO-treated SHSY5Y cells ± FT385 treatment (y-axis) and ± USP30 (x-axis). Mitochondrial (Integrated Mitochondrial Protein Index (IMPI) database; http://www.mrc-mbu.cam.ac.uk/impi; "known mitochondrial" only) and peroxisomal proteins (peroxisomeDB; http://www.peroxisomedb.org) proteins are highlighted in orange and purple respectively. Inset in (C) shows enlarged section of ubiquitylome data for peptides enriched in USP30 KO and inhibitor treated cells. Within proteome graphs (B) each dot represents a single protein identified by at least 2 peptides and the ratio shows the average of 2 experiments. Within ubiquitylome graphs (C) each dot represents a single diGly peptide (localisation ≥0.75) and the ratio shows the average of 2 experiments. (D) Heatmap showing diGly peptides that are increased consistently by $\log_2 \geq 0.8$ in both USP30 KO and USP30 inhibitor (FT385) treated cells. Grey indicates the protein was not seen in that condition, * indicates ambiguity of peptide assignment between family members (OSBPL3,OSBPL7,OSBPL6), # indicates an increase at proteome level in KO11. VDAC3 K53 and K54 correspond to equivalent lysines in two distinct isoforms. (E) Fold change ($\log_2$) in proteome and individual diGly peptides (localisation ≥0.75) by site in VDAC1 proteins. See Figure S3 for corresponding datasets for VDAC2 and 3 and proteome data for hits shown in D.

Figure 5. Proteomic analysis of the mitochondria-enriched ubiquitylome in USP30 KO SHSY5Y cells.

(A) Schematic flow-chart of SILAC based quantitative ubiquitylome and proteome analysis comparing two USP30-KO clones (KOD-sgRNA#1; KO11-sgRNA#2) to wild-type SHSY5Y cells. Cells were metabolically labelled by SILAC as shown and treated for 4 hours with AO (1 µM). Cells were then either lysed for total proteome analysis or further processed by subcellular fractionation. The mitochondrial fraction was used as the starting material for the ubiquitylome analysis.

(B) Graphs depicting the fold change (log_2) in the proteome of AO-treated USP30 KOD versus wild-type SHSY5Y (SH) (y-axis) and USP30 KO11 compared to SHSY5Y cells (x-axis). Mitochondrial (Integrated Mitochondrial Protein Index (IMPI) database; http://www.mrc-mbu.cam.ac.uk/impi; "known mitochondrial" only) and peroxisomal proteins (peroxisomeDB; http://www.peroxisomedb.org) proteins are highlighted in orange and purple respectively. Each dot represents a single protein identified by at least 2 peptides and the ratio shows the average of 3 experiments. (C) Heatmap showing diGly containing peptides that are increased consistently in at least 4 out of 6 experimental conditions by $log_2 \geq 0.8$. The corresponding data from the total ubiquitylome experiment shown in Figure 4 are also indicated. Grey indicates the protein was not seen in that condition. VDAC3 K53 and K54 correspond to equivalent lysines in two distinct isoforms. (D) Depiction of the localisation of USP30 sensitive depolarisation-induced ubiquitylated proteins within mitochondria (enriched proteins shown in C). Defined as outer mitochondrial membrane (green), inner mitochondrial membrane (blue) or matrix (pink).(E) Western blot showing the appearance of mono-ubiquitylated species of SYNJ2BP in both USP30 KO clones (KO11, KOD) and in USP30 inhibitor (FT385) treated cells. Cells were treated for 4 hours with AO (1 µM) in the presence or absence of 200 nM FT385, then lysed in Urea lysis buffer and analysed by western blot. Black and red arrowheads indicate unmodified and ubiquitylated SYN2BP (high exp. = higher exposure).

Figure 6. USP30 KO and USP30 Inhibition enhance phospho-Ser65 Ubiquitin levels on mitochondria of SHSY5Y cells.

(A) Comparison of depolarisation induced phosphoSer65-Ubiquitin (pUb) generation in SHSY5Y cells treated with FT385 and in USP30 KO SHSY5Y (KO11). Shown is a western blot and corresponding line-graph for the pUb signal, of lysates from cells treated for 4 hours with AO (1 µM) with or without FT385 (200 nM). Black and red arrowheads indicate unmodified and ubiquitylated TOM20 species respectively (high exp. = higher exposure). (B) Graph shows quantification of the pUb signal in the 17 to 76 kDa range for two independent experiments (A, and Figure S4A) with individual data points shown in dark and light blue. Error bars indicate the range. (C) A post-nuclear supernatant (PNS) and mitochondrial fractions (MF) were obtained from SHSY5Y cells treated in presence or absence of FT385 (100 nM, 24 hours), with DMSO or AO (1 µM). Samples were analysed by western blotting and a line graph depicting the pUb signal is shown. Bar chart shows quantification of the total pUb signal (left) and the pUb signal in the 38 to 76 kDa range (right). (D) SHSY5Y cells and two USP30 KO clones (KOD and KO11) were treated for 1 hour with AO (1 µM). Cells were homogenised and mitochondrial fractions (MF) prepared and analysed as indicated. Graphs show quantification of the total pUb signal and the ubiquitylated TOM20 (red arrowheads) normalised to unmodified TOM20 (black arrowheads) for two independent experiments with individual data points shown in dark and light blue. Error bars indicate the range. High exp. = higher exposure.

Figure 7. Working model depicting USP30 action upstream of PINK1. Under depolarising conditions PINK1 becomes activated but remains associated with TOM complex components. TOM complex associated ubiquitylation provides the nucleating substrate for PINK1-dependent phosphorylation of ubiquitin on Ser65. This leads to recruitment and activation of the E3 ligase Parkin, which can then amplify the signal. By opposing TOM complex ubiquitylation, USP30 suppresses the trigger for mitophagy.

Supplementary Figure legends

Figure S1 – sgRNA design for the generation of USP30 KO cell lines and sequence of the two SHSY5Y USP30 KO clones used in this study. KOD and KOC were generated using sgRNA#1 (target region shown in orange) and KO11 was generated using sgRNA#2 (target region shown in blue). Insertions and deletions are indicated in red. TSS: transcriptional start site. The green codon corresponds to catalytic C77. Frequency of allele detection: KOD allele 1 (7/10), allele 2 (3/10); KOC allele 1 (5/10), allele 2 (5/10); KO11 allele 1 (4/5), allele 2 (1/5).

Figure S2 – USP30 KO enhances depolarisation induced ubiquitylation of TOM20.
(A) SHSY5Y and two independent USP30 KO clones (KOC and KOD) were treated for 4 and 8 hours with Antimycin A and Oligomycin A (AO; 1 µM each) or DMSO, lysed and analysed by western blotting. (B-C) Graphs show quantification of ubiquitylated species of MFN2 and TOM20 normalised to the unmodified counterparts. (D) SHSY5Y cells and two USP30 KO clones (KOD and KO11) were treated for 1 and 4 hours with AO (1 µM). Cells were homogenised and mitochondrial fractions (MF) prepared and analysed as indicated. Bar charts show quantification of (E) ubiquitylated TOM20 normalised to unmodified TOM20 and (F) PINK1. Black and red arrowheads indicate unmodified and ubiquitylated MFN2, TOM20 and FIS1 respectively (high exp. = higher exposure).

Figure S3 – Ubiquitylome and total proteome changes in USP30 KO versus USP30 inhibitor treated SHSY5Y cells. (A,B) Fold change ($\log_2$) in proteome and individual diGly peptides (localisation ≥0.75) by site in VDAC2 and VDAC3 proteins.(C) Annotated version of the graph shown in Figure 4C depicting the fold change ($\log_2$) in the ubiquitylome of AO-treated SHSY5Y cells ± FT385 treatment (y-axis) and ± USP30 (x-axis). Each dot represents a single diGly peptide (localisation ≥0.75) and the ratio shows the average of 2 experiments. In green are shown diGly peptides that are increased consistently by $\log_2 \geq 0.8$ in both USP30 inhibitor (FT385) treated but not in either USP30 KO11 datasets. Labelled are those diGly peptides that pass a $\log_2 \geq 1.2$ threshold in both FT385 conditions. * indicates ambiguity of peptide assignment between family members (AMMECR1L, AMMECR1 and PCDHB3, PCDHB2). (D,E) Heat maps show total proteome data corresponding to the ubiquitylated peptides highlighted in Figures 4D and 5C respectively. Grey indicates the protein was not seen in that condition.

Figure S4 – Comparison of depolarisation induced phosphoSer65-Ubiquitin (pUb) generation in SHSY5Y cells treated with FT385 and USP30 KO SHSY5Y (KO11 and KOD). (A) western blot of the same samples shown in Figure 3C, and corresponding line-graph for the pUb signal, of lysates from cells treated for 4 hours with AO (1 µM) with or without FT385 (200 nM). (B) Same samples as in Figure 6A probed for total ubiquitin (VU1).

Supplementary Tables:

Table S1. Proteome and ubiquitylome data for USP30 KO and inhibitor treated SHSY5Y cells. Comparisons with AO and/or inhibitor are 24 hours post treatment (AO = 1 µM, FT385=200 nM). Data relate to figure 4.

Table S2. Total Proteome and Mitochondrial-enriched ubiquitylome data for USP30 Knockout SHSY5Y cells (Clones KO11 and KOD) compared to WT. All conditions were subject to depolarisation (AO 1 µM) for 4 hours. Data relate to figure 5.

Bibliography

Allen, G.F., R. Toth, J. James, and I.G. Ganley. 2013. Loss of iron triggers PINK1/Parkin-independent mitophagy. *EMBO Rep*. 14:1127-1135.
Aubry, L., and G. Klein. 2006. Purification techniques of subcellular compartments for analytical and preparative purposes. *Methods Mol Biol*. 346:171-185.
Barneo-Munoz, M., P. Juarez, A. Civera-Tregon, L. Yndriago, D. Pla-Martin, J. Zenker, C. Cuevas-Martin, A. Estela, M. Sanchez-Arago, J. Forteza-Vila, et al. 2015. Lack of GDAP1 induces neuronal calcium and mitochondrial defects in a knockout mouse model of charcot-marie-tooth neuropathy. *PLoS Genet*. 11:e1005115.
Barretina, J., G. Caponigro, N. Stransky, K. Venkatesan, A.A. Margolin, S. Kim, C.J. Wilson, J. Lehar, G.V. Kryukov, D. Sonkin, et al. 2012. The Cancer Cell Line Encyclopedia enables predictive modelling of anticancer drug sensitivity. *Nature*. 483:603-607.
Bashore, C., P. Jaishankar, N.J. Skelton, J. Fuhrmann, B.R. Hearn, P.S. Liu, A.R. Renslo, and E.C. Dueber. 2020. Cyanopyrrolidine Inhibitors of Ubiquitin Specific Protease 7 Mediate Desulfhydration of the Active-Site Cysteine. *ACS Chem Biol*.
Bingol, B., and M. Sheng. 2016. Mechanisms of mitophagy: PINK1, Parkin, USP30 and beyond. *Free Radic Biol Med*. 100:210-222.
Bingol, B., J.S. Tea, L. Phu, M. Reichelt, C.E. Bakalarski, Q. Song, O. Foreman, D.S. Kirkpatrick, and M. Sheng. 2014. The mitochondrial deubiquitinase USP30 opposes parkin-mediated mitophagy. *Nature*. 510:370-375.
Bravo-San Pedro, J.M., G. Kroemer, and L. Galluzzi. 2017. Autophagy and Mitophagy in Cardiovascular Disease. *Circ Res*. 120:1812-1824.
Clague, M.J., I. Barsukov, J.M. Coulson, H. Liu, D.J. Rigden, and S. Urbe. 2013. Deubiquitylases from genes to organism. *Physiol Rev*. 93:1289-1315.
Clague, M.J., and S. Urbe. 2017. Integration of cellular ubiquitin and membrane traffic systems: focus on deubiquitylases. *FEBS J*. 284:1753-1766.
Clague, M.J., S. Urbe, and D. Komander. 2019. Breaking the chains: deubiquitylating enzyme specificity begets function. *Nat Rev Mol Cell Biol*. 20:338-352.
Cunningham, C.N., J.M. Baughman, L. Phu, J.S. Tea, C. Yu, M. Coons, D.S. Kirkpatrick, B. Bingol, and J.E. Corn. 2015. USP30 and parkin homeostatically regulate atypical ubiquitin chains on mitochondria. *Nat Cell Biol*. 17:160-169.
Davis, S., P.D. Charles, L. He, P. Mowlds, B.M. Kessler, and R. Fischer. 2017. Expanding Proteome Coverage with CHarge Ordered Parallel Ion aNalysis (CHOPIN) Combined with Broad Specificity Proteolysis. *J Proteome Res*. 16:1288-1299.
Ekkebus, R., D. Flierman, P.P. Geurink, and H. Ovaa. 2014. Catching a DUB in the act: novel ubiquitin-based active site directed probes. *Curr Opin Chem Biol*. 23:63-70.
Fritsch, L.E., M.E. Moore, S.A. Sarraf, and A.M. Pickrell. 2019. Ubiquitin and Receptor Dependent Mitophagy Pathways and Their Implication in Neurodegeneration. *J Mol Biol*.
Gavory, G., C.R. O'Dowd, M.D. Helm, J. Flasz, E. Arkoudis, A. Dossang, C. Hughes, E. Cassidy, K. McClelland, E. Odrzywol, et al. 2018. Discovery and characterization of highly potent and selective allosteric USP7 inhibitors. *Nat Chem Biol*. 14:118-125.
Gersch, M., C. Gladkova, A.F. Schubert, M.A. Michel, S. Maslen, and D. Komander. 2017. Mechanism and regulation of the Lys6-selective deubiquitinase USP30. *Nat Struct Mol Biol*. 24:920-930.
Gladkova, C., S.L. Maslen, J.M. Skehel, and D. Komander. 2018. Mechanism of parkin activation by PINK1. *Nature*. 559:410-414.
Gold, V.A., P. Chroscicki, P. Bragoszewski, and A. Chacinska. 2017. Visualization of cytosolic ribosomes on the surface of mitochondria by electron cryo-tomography. *EMBO Rep*. 18:1786-1800.
Harper, J.W., A. Ordureau, and J.M. Heo. 2018. Building and decoding ubiquitin chains for mitophagy. *Nat Rev Mol Cell Biol*. 19:93-108.
Hart, T., A.H.Y. Tong, K. Chan, J. Van Leeuwen, A. Seetharaman, M. Aregger, M. Chandrashekhar, N. Hustedt, S. Seth, A. Noonan, A. Habsid, O. Sizova, L. Nedyalkova, R. Climie, L. Tworzyanski, K. Lawson, M.A. Sartori, S. Alibeh, et al. 2017. Evaluation and Design of Genome-Wide CRISPR/SpCas9 Knockout Screens. *G3 (Bethesda)*. 7:2719-2727.

Hewings, D.S., J. Heideker, T.P. Ma, A.P. AhYoung, F. El Oualid, A. Amore, G.T. Costakes, D. Kirchhofer, B. Brasher, T. Pillow, et al. 2018. Reactive-site-centric chemoproteomics identifies a distinct class of deubiquitinase enzymes. *Nat Commun*. 9:1162.
Hoshino, A., W.J. Wang, S. Wada, C. McDermott-Roe, C.S. Evans, B. Gosis, M.P. Morley, K.S. Rathi, J. Li, K. Li, et al. 2019. The ADP/ATP translocase drives mitophagy independent of nucleotide exchange. *Nature*. 575:375-379.
Jin, S.M., and R.J. Youle. 2013. The accumulation of misfolded proteins in the mitochondrial matrix is sensed by PINK1 to induce PARK2/Parkin-mediated mitophagy of polarized mitochondria. *Autophagy*. 9:1750-1757.
Joazeiro, C.A.P. 2017. Ribosomal Stalling During Translation: Providing Substrates for Ribosome-Associated Protein Quality Control. *Annu Rev Cell Dev Biol*. 33:343-368.
Kane, L.A., M. Lazarou, A.I. Fogel, Y. Li, K. Yamano, S.A. Sarraf, S. Banerjee, and R.J. Youle. 2014. PINK1 phosphorylates ubiquitin to activate Parkin E3 ubiquitin ligase activity. *J Cell Biol*. 205:143-153.
Kategaya, L., P. Di Lello, L. Rouge, R. Pastor, K.R. Clark, J. Drummond, T. Kleinheinz, E. Lin, J.P. Upton, S. Prakash, et al. 2017. USP7 small-molecule inhibitors interfere with ubiquitin binding. *Nature*. 550:534-538.
Kazlauskaite, A., V. Kelly, C. Johnson, C. Baillie, C.J. Hastie, M. Peggie, T. Macartney, H.I. Woodroof, D.R. Alessi, P.G. Pedrioli, and M.M. Muqit. 2014a. Phosphorylation of Parkin at Serine65 is essential for activation: elaboration of a Miro1 substrate-based assay of Parkin E3 ligase activity. *Open Biol*. 4:130213.
Kazlauskaite, A., C. Kondapalli, R. Gourlay, D.G. Campbell, M.S. Ritorto, K. Hofmann, D.R. Alessi, A. Knebel, M. Trost, and M.M. Muqit. 2014b. Parkin is activated by PINK1-dependent phosphorylation of ubiquitin at Ser65. *Biochem J*. 460:127-139.
Kluge, A.F., B.R. Lagu, P. Maiti, M. Jaleel, M. Webb, J. Malhotra, A. Mallat, P.A. Srinivas, and J.E. Thompson. 2018. Novel highly selective inhibitors of ubiquitin specific protease 30 (USP30) accelerate mitophagy. *Bioorg Med Chem Lett*. 28:2655-2659.
Koyano, F., K. Okatsu, H. Kosako, Y. Tamura, E. Go, M. Kimura, Y. Kimura, H. Tsuchiya, H. Yoshihara, T. Hirokawa, et al. 2014. Ubiquitin is phosphorylated by PINK1 to activate parkin. *Nature*. 510:162-166.
Kuroha, K., A. Zinoviev, C.U.T. Hellen, and T.V. Pestova. 2018. Release of Ubiquitinated and Non-ubiquitinated Nascent Chains from Stalled Mammalian Ribosomal Complexes by ANKZF1 and Ptrh1. *Mol Cell*. 72:286-302 e288.
Laine, D., M. Palovich, B. McCleland, E. Petitjean, I. Delhom, H. Xie, J. Deng, G. Lin, R. Davis, A. Jolit, etal. 2011. Discovery of novel cyanamide-based inhibitors of cathepsin C. *ACS Med Chem Lett*. 2:142-147.
Lamberto, I., X. Liu, H.S. Seo, N.J. Schauer, R.E. Iacob, W. Hu, D. Das, T. Mikhailova, E.L. Weisberg, J.R. Engen,et al. 2017. Structure-Guided Development of a Potent and Selective Non-covalent Active-Site Inhibitor of USP7. *Cell Chem Biol*. 24:1490-1500.
Lavie, J., H. De Belvalet, S. Sonon, A.M. Ion, E. Dumon, S. Melser, D. Lacombe, J.W. Dupuy, C. Lalou, and G. Benard. 2018. Ubiquitin-Dependent Degradation of Mitochondrial Proteins Regulates Energy Metabolism. *Cell Rep*. 23:2852-2863.
Lazarou, M., S.M. Jin, L.A. Kane, and R.J. Youle. 2012. Role of PINK1 binding to the TOM complex and alternate intracellular membranes in recruitment and activation of the E3 ligase Parkin. *Dev Cell*. 22:320-333.
Lee, M.J., B.H. Lee, J. Hanna, R.W. King, and D. Finley. 2011. Trimming of ubiquitin chains by proteasome-associated deubiquitinating enzymes. *Mol Cell Proteomics*. 10:R110.003871.
Liang, J.R., A. Martinez, J.D. Lane, U. Mayor, M.J. Clague, and S. Urbe. 2015. USP30 deubiquitylates mitochondrial Parkin substrates and restricts apoptotic cell death. *EMBO Rep*. 16:618-627.
Marcassa, E., A. Kallinos, J. Jardine, E.V. Rusilowicz-Jones, A. Martinez, S. Kuehl, M. Islinger, M.J. Clague, and S. Urbe. 2018. Dual role of USP30 in controlling basal pexophagy and mitophagy. *EMBO Rep*. 19:e45595.
Meyers, R.M., J.G. Bryan, J.M. McFarland, B.A. Weir, A.E. Sizemore, H. Xu, N.V. Dharia, P.G. Montgomery, G.S. Cowley, S. Pantel, et al. 2017. Computational correction of copy number effect improves specificity of CRISPR-Cas9 essentiality screens in cancer cells. *Nat Genet*. 49:1779-1784.
Miller, S., and M.M.K. Muqit. 2019. Therapeutic approaches to enhance PINK1/Parkin mediated mitophagy for the treatment of Parkinson's disease. *Neurosci Lett*. 705:7-13.
Montava-Garriga, L., F. Singh, G. Ball, and I.G. Ganley. 2020. Semi-automated quantitation of mitophagy in cells and tissues. *Mech Ageing Dev*. 185:111196.

Nakamura, N., and S. Hirose. 2008. Regulation of Mitochondrial Morphology by USP30, a Deubiquitinating Enzyme Present in the Mitochondrial Outer Membrane. *Mol Biol Cell*. 19:1903-1911.
Nemoto, Y., and P. De Camilli. 1999. Recruitment of an alternatively spliced form of synaptojanin 2 to mitochondria by the interaction with the PDZ domain of a mitochondrial outer membrane protein. *EMBO J*. 18:2991-3006.
Okatsu, K., M. Kimura, T. Oka, K. Tanaka, and N. Matsuda. 2015. Unconventional PINK1 localization to the outer membrane of depolarized mitochondria drives Parkin recruitment. *J Cell Sci*. 128:964-978.
Okatsu, K., M. Uno, F. Koyano, E. Go, M. Kimura, T. Oka, K. Tanaka, and N. Matsuda. 2013. A dimeric PINK1-containing complex on depolarized mitochondria stimulates Parkin recruitment. *J Biol Chem*. 288:36372-36384.
Ordureau, A., J.A. Paulo, J. Zhang, H. An, K.N. Swatek, J.R. Cannon, Q. Wan, D. Komander, and J.W. Harper. 2020. Global Landscape and Dynamics of Parkin and USP30-Dependent Ubiquitylomes in iNeurons during Mitophagic Signaling. *Mol Cell*. 77:1124-1142 e1110.
Ordureau, A., J.A. Paulo, W. Zhang, T. Ahfeldt, J. Zhang, E.F. Cohn, Z. Hou, J.M. Heo, L.L. Rubin, S.S. Sidhu, et al. 2018. Dynamics of PARKIN-Dependent Mitochondrial Ubiquitylation in Induced Neurons and Model Systems Revealed by Digital Snapshot Proteomics. *Mol Cell*. 70:211-227 e218.
Ordureau, A., S.A. Sarraf, D.M. Duda, J.M. Heo, M.P. Jedrychowski, V.O. Sviderskiy, J.L. Olszewski, J.T. Koerber, T. Xie, S.A. Beausoleil, et al. 2014. Quantitative Proteomics Reveal a Feedforward Mechanism for Mitochondrial PARKIN Translocation and Ubiquitin Chain Synthesis. *Mol Cell*. 56:360-375.
Peng, J., D. Schwartz, J.E. Elias, C.C. Thoreen, D. Cheng, G. Marsischky, J. Roelofs, D. Finley, and S.P. Gygi. 2003. A proteomics approach to understanding protein ubiquitination. *Nat Biotechnol*. 21:921-926.
Phu, L., C.M. Rose, J.S. Tea, C.E. Wall, E. Verschueren, T.K. Cheung, D.S. Kirkpatrick, and B. Bingol. 2020. Dynamic Regulation of Mitochondrial Import by the Ubiquitin System. *Mol Cell*. 77:1107-1123 e1110.
Pickles, S., P. Vigie, and R.J. Youle. 2018. Mitophagy and Quality Control Mechanisms in Mitochondrial Maintenance. *Curr Biol*. 28:R170-R185.
Pickrell, A.M., and R.J. Youle. 2015. The roles of PINK1, parkin, and mitochondrial fidelity in Parkinson's disease. *Neuron*. 85:257-273.
Pinto-Fernandez, A., S. Davis, A.B. Schofield, H.C. Scott, P. Zhang, E. Salah, S. Mathea, P.D. Charles, A. Damianou, G. Bond, et al. 2019. Comprehensive Landscape of Active Deubiquitinating Enzymes Profiled by Advanced Chemoproteomics. *Front Chem*. 7:592.
Rakovic, A., K. Shurkewitsch, P. Seibler, A. Grunewald, A. Zanon, J. Hagenah, D. Krainc, and C. Klein. 2013. Phosphatase and tensin homolog (PTEN)-induced putative kinase 1 (PINK1)-dependent ubiquitination of endogenous Parkin attenuates mitophagy: study in human primary fibroblasts and induced pluripotent stem cell-derived neurons. *J Biol Chem*. 288:2223-2237.
Riccio, V., N. Demers, R. Hua, M. Vissa, D.T. Cheng, A.W. Strilchuk, Y. Wang, G.A. McQuibban, and P.K. Kim. 2019. Deubiquitinating enzyme USP30 maintains basal peroxisome abundance by regulating pexophagy. *J Cell Biol*. 218:798-807.
Ritorto, M.S., R. Ewan, A.B. Perez-Oliva, A. Knebel, S.J. Buhrlage, M. Wightman, S.M. Kelly, N.T. Wood, S. Virdee, N.S. Gray,et al. 2014. Screening of DUB activity and specificity by MALDI-TOF mass spectrometry. *Nat Commun*. 5:4763.
Sarraf, S.A., M. Raman, V. Guarani-Pereira, M.E. Sowa, E.L. Huttlin, S.P. Gygi, and J.W. Harper. 2013. Landscape of the PARKIN-dependent ubiquitylome in response to mitochondrial depolarization. *Nature*. 496:372-376.
Schauer, N., R.S. Magin, X. Liu, L. Doherty, and S. Buhrlage. 2019. Advances in Discovering Deubiquitinating Enzyme (DUB) Inhibitors. *J Med Chem*.
Sekine, S., and R.J. Youle. 2018. PINK1 import regulation; a fine system to convey mitochondrial stress to the cytosol. *BMC Biol*. 16:2.
Sorrentino, V., M. Romani, L. Mouchiroud, J.S. Beck, H. Zhang, D. D'Amico, N. Moullan, F. Potenza, A.W. Schmid, S. Rietsch, et al. 2017. Enhancing mitochondrial proteostasis reduces amyloid-beta proteotoxicity. *Nature*. 552:187-193.
Tsubouchi, K., J. Araya, and K. Kuwano. 2018. PINK1-PARK2-mediated mitophagy in COPD and IPF pathogeneses. *Inflamm Regen*. 38:18.

Turnbull, A.P., S. Ioannidis, W.W. Krajewski, A. Pinto-Fernandez, C. Heride, A.C.L. Martin, L.M. Tonkin, E.C. Townsend, S.M. Buker, D.R. Lancia, et al. 2017. Molecular basis of USP7 inhibition by selective small-molecule inhibitors. *Nature*. 550:481-486.
Tyanova, S., T. Temu, and J. Cox. 2016. The MaxQuant computational platform for mass spectrometry-based shotgun proteomics. *Nat Protoc*. 11:2301-2319.
Urbe, S., H. Liu, S.D. Hayes, C. Heride, D.J. Rigden, and M.J. Clague. 2012. Systematic survey of deubiquitinase localisation identifies USP21 as a regulator of centrosome and microtubule associated functions. *Mol Biol Cell*. 23:1095-1103.
Wauer, T., M. Simicek, A. Schubert, and D. Komander. 2015a. Mechanism of phospho-ubiquitin-induced PARKIN activation. *Nature*. 524:370-374.
Wauer, T., K.N. Swatek, J.L. Wagstaff, C. Gladkova, J.N. Pruneda, M.A. Michel, M. Gersch, C.M. Johnson, S.M. Freund, and D. Komander. 2015b. Ubiquitin Ser65 phosphorylation affects ubiquitin structure, chain assembly and hydrolysis. *EMBO J*. 34:307-325.
Wiedemann, N., and N. Pfanner. 2017. Mitochondrial Machineries for Protein Import and Assembly. *Annu Rev Biochem*. 86:685-714.

A

FT3967385 (FT385)

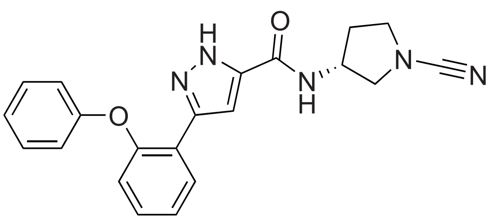

B

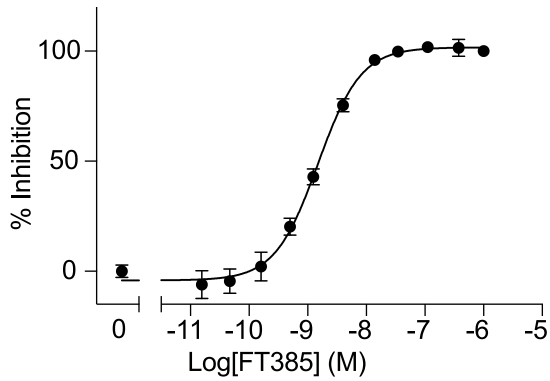

C

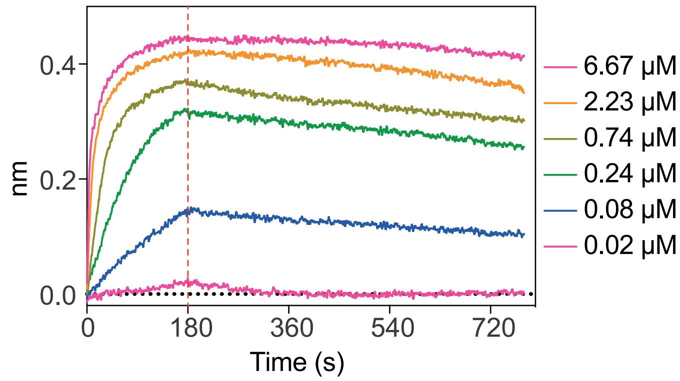

D

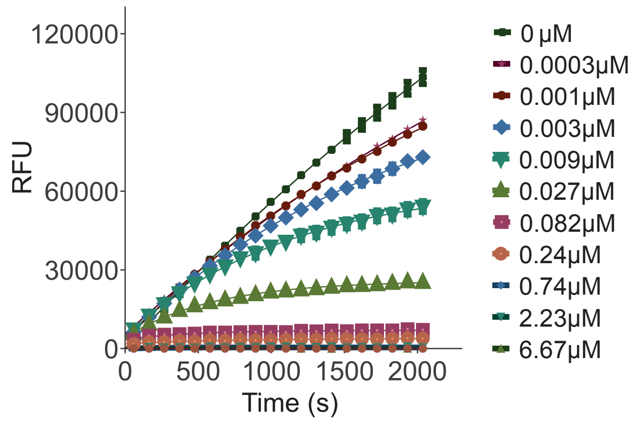

E

FT385	
IC_{50} (B)	1.5nM
k_{on} (C)	3.09 x 10^4 M^{-1} s^{-1}
K_I (D)	0.014 µM
k_{inact} (D)	0.0025 s^{-1}
k_{inact}/K_I (D)	0.18 s^{-1} $µM^{-1}$

F

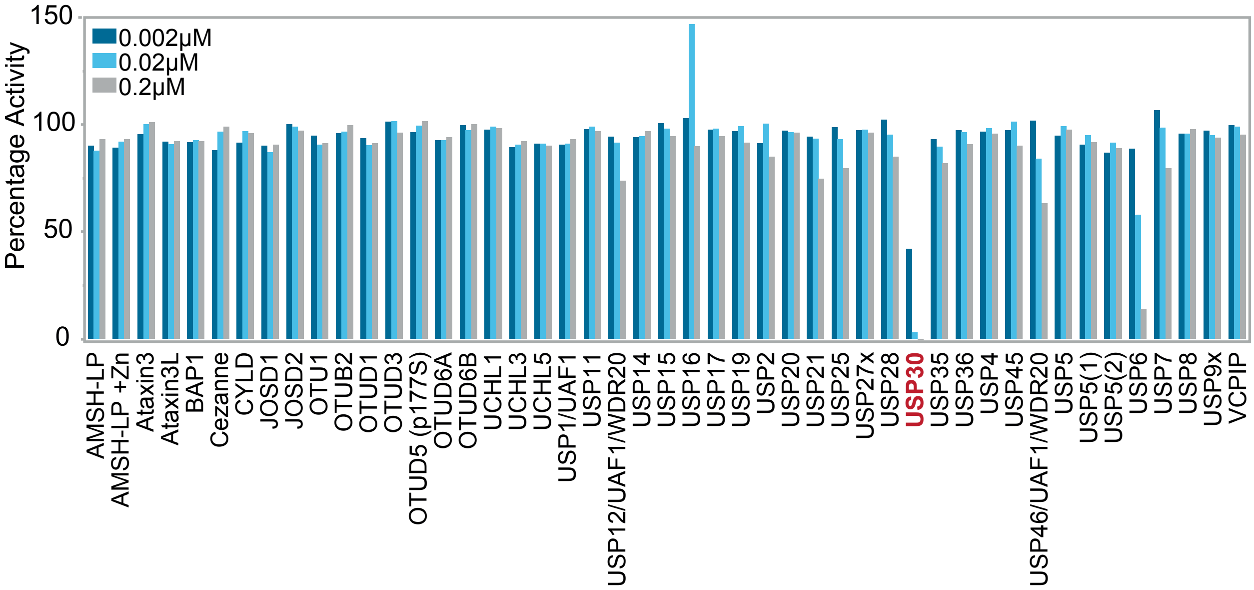

Figure 1

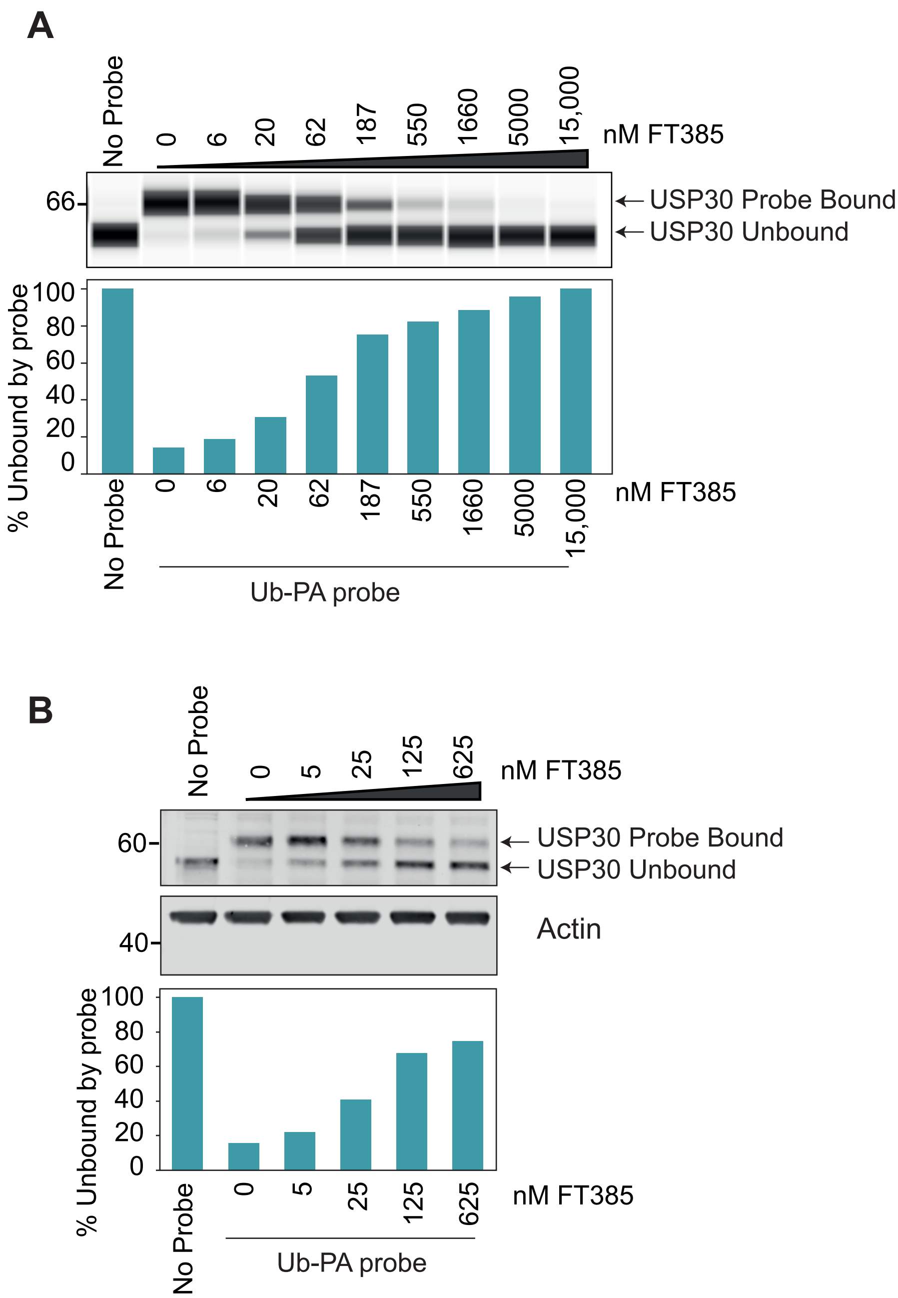
A
No Probe
0
6
20
62
187
550
1660
5000
15,000
nM FT385
66
USP30 Probe Bound
USP30 Unbound
% Unbound by probe
100
80
60
40
20
0
Ub-PA probe
B
No Probe
0
5
25
125
625
nM FT385
60
USP30 Probe Bound
USP30 Unbound
Actin
40
% Unbound by probe
Ub-PA probe

Figure 2

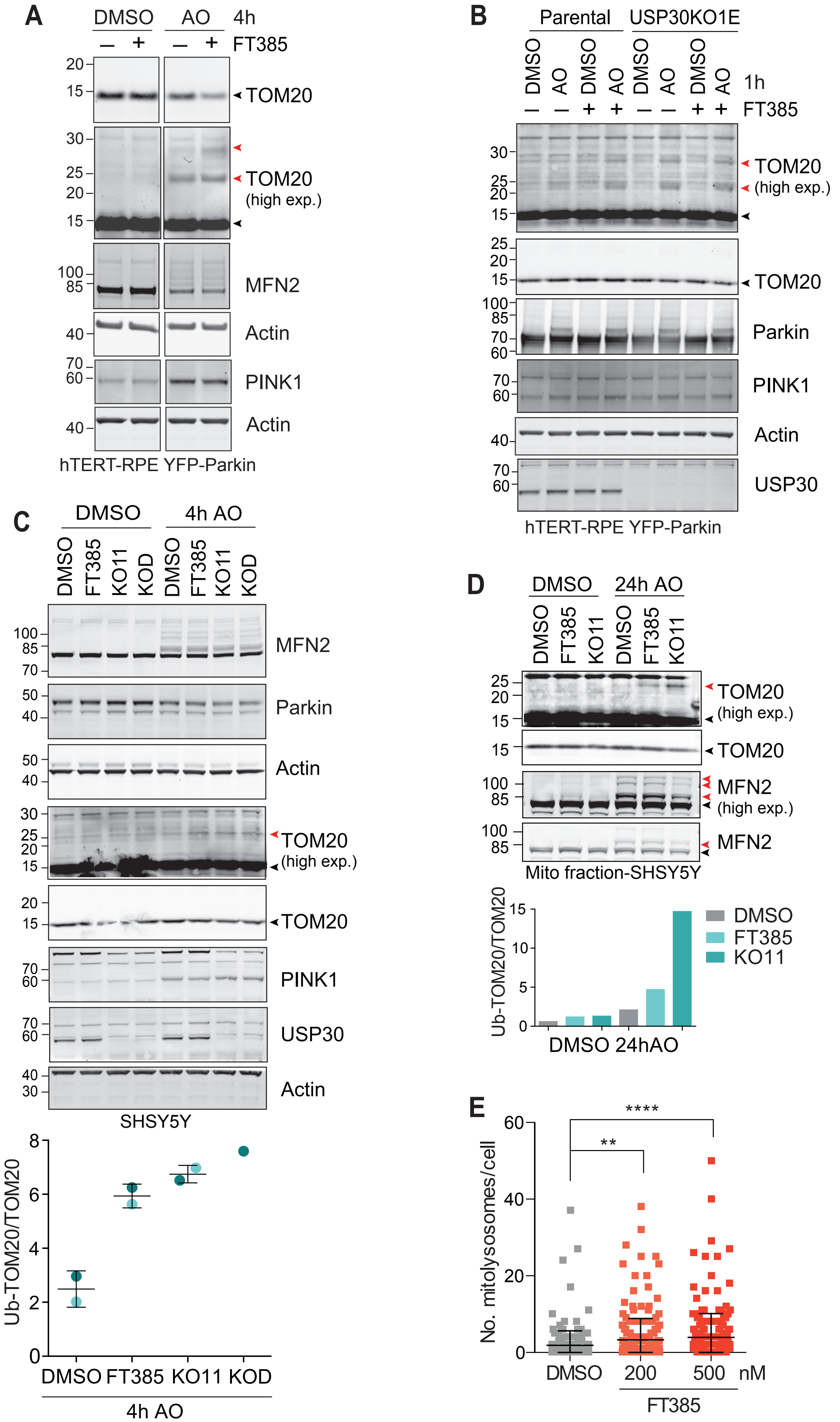
A
DMSO
AO
4h
FT385
TOM20
TOM20
(high exp.)
MFN2
Actin
PINK1
Actin
hTERT-RPE YFP-Parkin
B
Parental
USP30KO1E
1h
FT385
TOM20
(high exp.)
TOM20
Parkin
PINK1
Actin
USP30
hTERT-RPE YFP-Parkin
C
DMSO
4h AO
FT385
KO11
KOD
MFN2
Parkin
Actin
TOM20
(high exp.)
TOM20
PINK1
USP30
Actin
SHSY5Y
Ub-TOM20/TOM20
4h AO
D
DMSO
24h AO
TOM20
(high exp.)
TOM20
MFN2
(high exp.)
MFN2
Mito fraction-SHSY5Y
Ub-TOM20/TOM20
DMSO 24hAO
E
No. mitolysosomes/cell
****
**
DMSO
200
500
nM
FT385

Figure 3

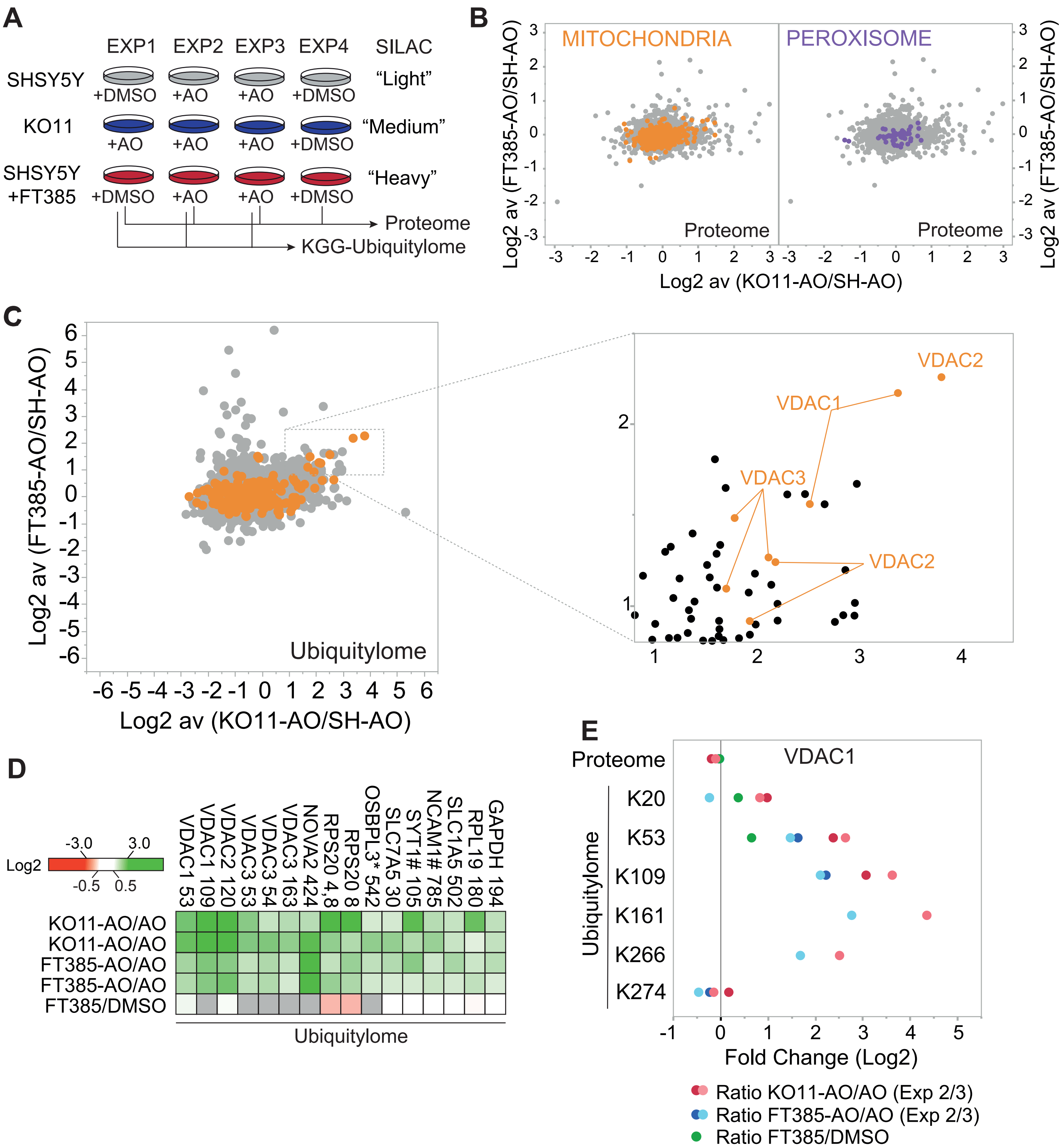
A
EXP1 EXP2 EXP3 EXP4 SILAC
SHSY5Y
+DMSO +AO +AO +DMSO
"Light"
KO11
+AO +AO +AO +DMSO
"Medium"
SHSY5Y +FT385
+DMSO +AO +AO +DMSO
"Heavy"
Proteome
KGG-Ubiquitylome
B
MITOCHONDRIA
PEROXISOME
Proteome
Log2 av (FT385-AO/SH-AO)
Log2 av (KO11-AO/SH-AO)
C
Ubiquitylome
Log2 av (FT385-AO/SH-AO)
Log2 av (KO11-AO/SH-AO)
VDAC2
VDAC1
VDAC3
D
Log2
-3.0 3.0
-0.5 0.5
VDAC1 53
VDAC1 109
VDAC2 120
VDAC3 53
VDAC3 54
VDAC3 163
NOVA2 424
RPS20 4,8
RPS20 8
OSBPL3* 542
SLC7A5 30
SYT1# 105
NCAM1# 785
SLC1A5 502
RPL19 180
GAPDH 194
KO11-AO/AO
KO11-AO/AO
FT385-AO/AO
FT385-AO/AO
FT385/DMSO
Ubiquitylome
E
VDAC1
Proteome
Ubiquitylome
K20
K53
K109
K161
K266
K274
Fold Change (Log2)
Ratio KO11-AO/AO (Exp 2/3)
Ratio FT385-AO/AO (Exp 2/3)
Ratio FT385/DMSO

Figure 4

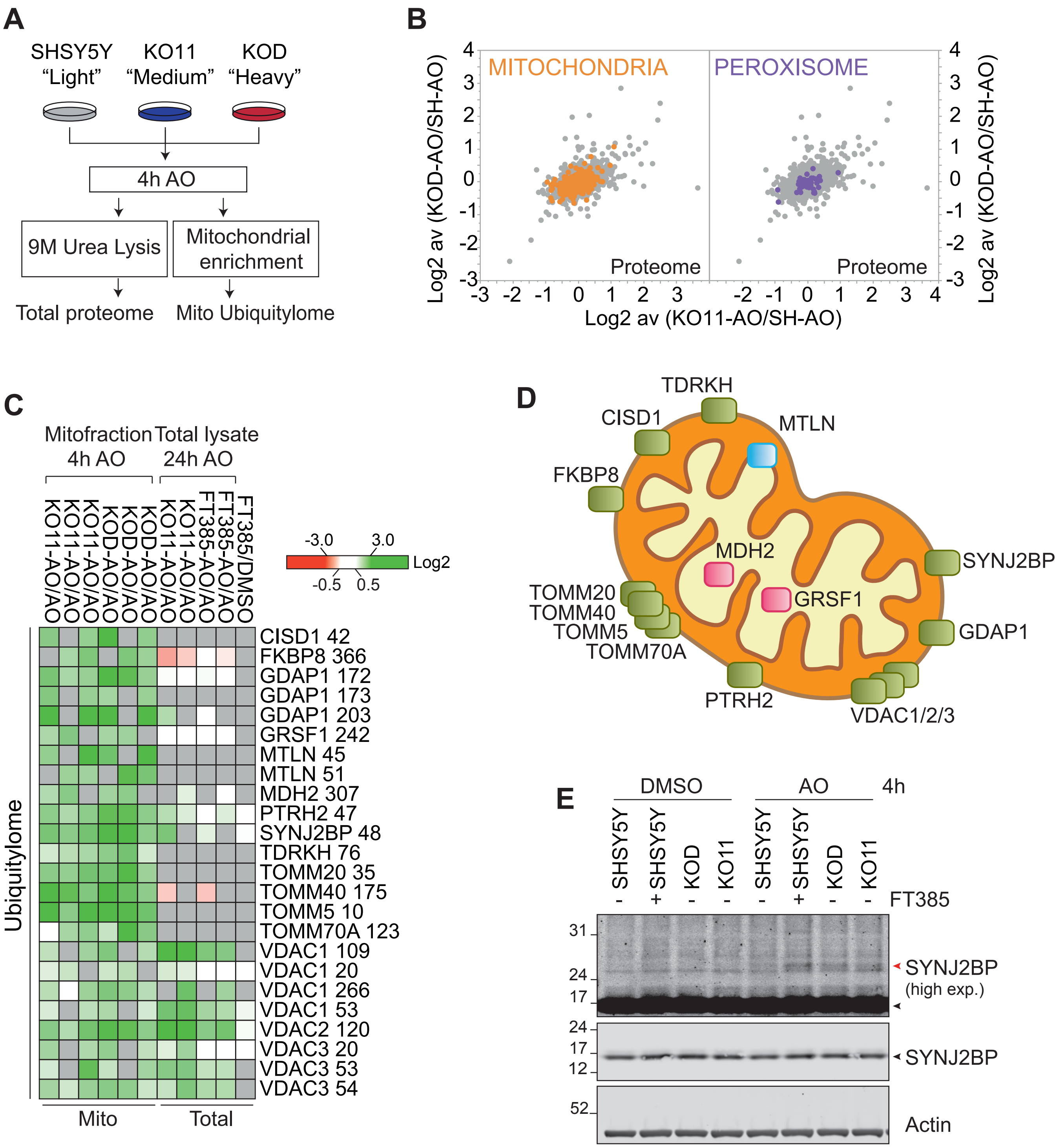
A
SHSY5Y "Light"
KO11 "Medium"
KOD "Heavy"
4h AO
9M Urea Lysis
Mitochondrial enrichment
Total proteome
Mito Ubiquitylome
B
MITOCHONDRIA
PEROXISOME
Proteome
Proteome
Log2 av (KOD-AO/SH-AO)
Log2 av (KO11-AO/SH-AO)
C
Mitofraction 4h AO
Total lysate 24h AO
KO11-AO/AO
KO11-AO/AO
KO11-AO/AO
KOD-AO/AO
KOD-AO/AO
KOD-AO/AO
KO11-AO/AO
KO11-AO/AO
FT385-AO/AO
FT385-AO/AO
FT385/DMSO
-3.0
3.0
-0.5
0.5
Log2
Ubiquitylome
CISD1 42
FKBP8 366
GDAP1 172
GDAP1 173
GDAP1 203
GRSF1 242
MTLN 45
MTLN 51
MDH2 307
PTRH2 47
SYNJ2BP 48
TDRKH 76
TOMM20 35
TOMM40 175
TOMM5 10
TOMM70A 123
VDAC1 109
VDAC1 20
VDAC1 266
VDAC1 53
VDAC2 120
VDAC3 20
VDAC3 53
VDAC3 54
Mito
Total
D
TDRKH
CISD1
MTLN
FKBP8
MDH2
SYNJ2BP
TOMM20
TOMM40
TOMM5
TOMM70A
GRSF1
GDAP1
PTRH2
VDAC1/2/3
E
DMSO
AO
4h
SHSY5Y
SHSY5Y
KOD
KO11
SHSY5Y
SHSY5Y
KOD
KO11
FT385
31
24
17
SYNJ2BP (high exp.)
24
17
12
SYNJ2BP
52
Actin

Figure 5

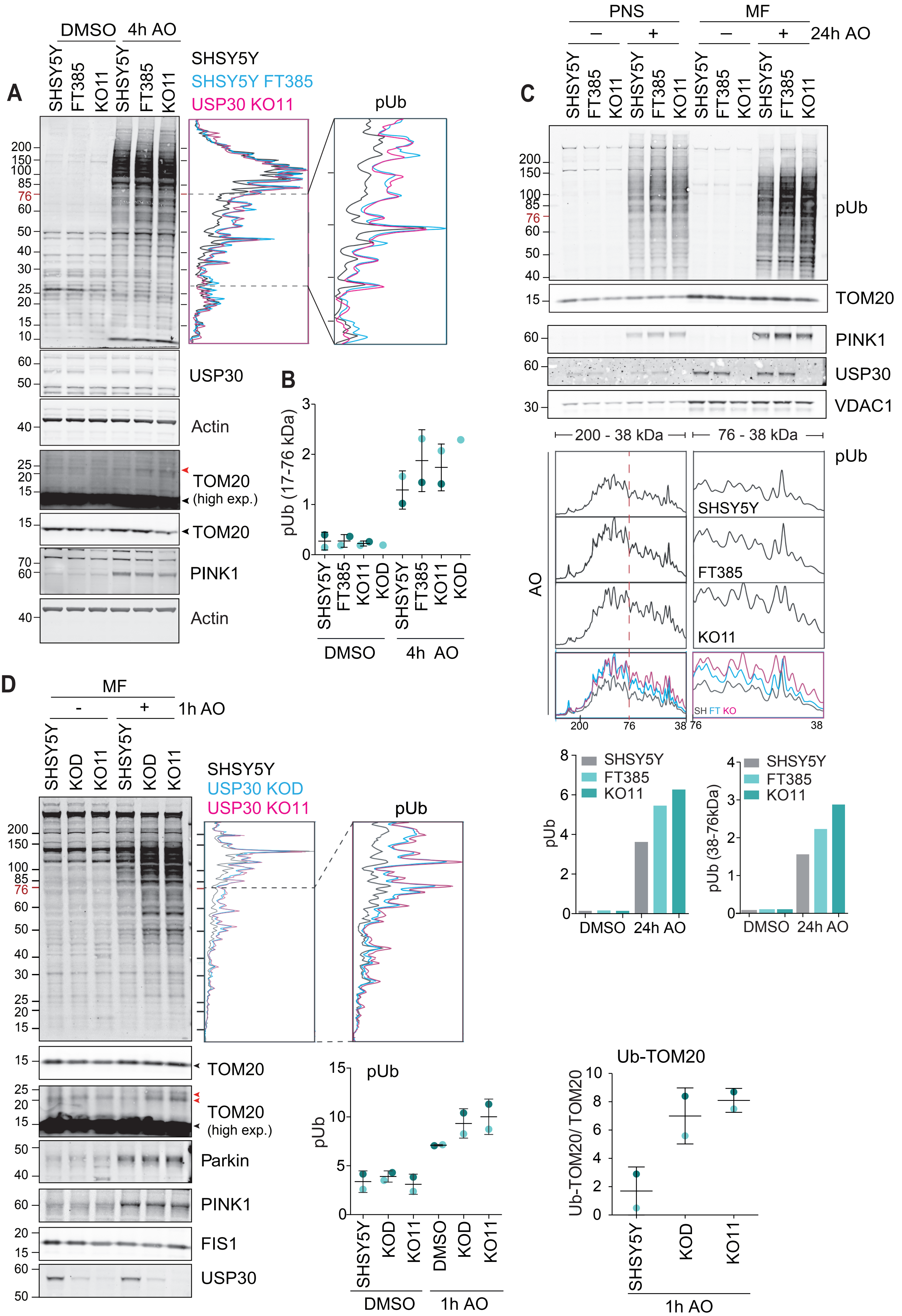
A
DMSO
4h AO
SHSY5Y
FT385
KO11
SHSY5Y
SHSY5Y FT385
USP30 KO11
pUb
USP30
Actin
TOM20
(high exp.)
TOM20
PINK1
Actin
B
pUb (17-76 kDa)
SHSY5Y
FT385
KO11
KOD
DMSO
4h AO
C
PNS
MF
24h AO
pUb
TOM20
PINK1
USP30
VDAC1
200 - 38 kDa
76 - 38 kDa
AO
SHSY5Y
FT385
KO11
SH FT KO
pUb
pUb (38-76kDa)
DMSO
24h AO
D
MF
1h AO
SHSY5Y
KOD
KO11
SHSY5Y
USP30 KOD
USP30 KO11
pUb
TOM20
TOM20
(high exp.)
Parkin
PINK1
FIS1
USP30
pUb
DMSO
1h AO
Ub-TOM20
Ub-TOM20/ TOM20
SHSY5Y
KOD
KO11
1h AO

Figure 6

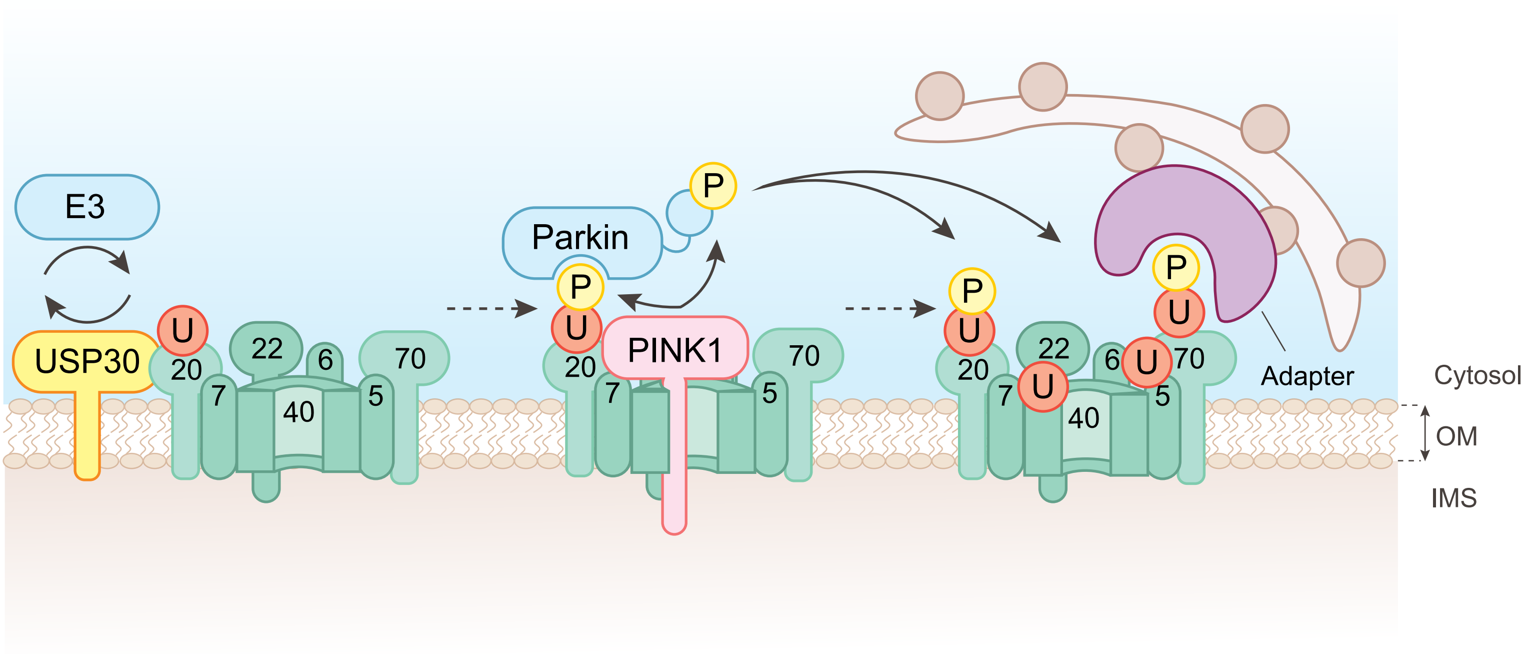

E3
USP30
U
20
22
6
7
40
5
70
Parkin
P
P
U
20
PINK1
7
5
70
P
U
20
22
6
U
70
7
U
40
5
P
U
Adapter
Cytosol
OM
IMS

Figure 7

```
Reference 1    GCCTGTCCTGCTTTCATCAGGTGGCTGGAAGAGTTCACCTCCCAGTACTCCAGGGATCAG TSS +261
KOD-allele 1   GCCTGTCCTGCTTTCATCAGGTGGCTGGAAGAGTTCACCTCCCAGTAC-------ATCAG     -7nt
KOD-allele 2   GCCTGTCCTGCTTTCATCAGGTGGCTGGAAGAGTTCACCTCCCAGT-------------G    -13nt

Reference 1    GCCTGTCCTGCTTTCATCAGGTGGCTGGAAGAGTTCACCTCCCAGTACTCCAGGGATCAG TSS +261
KOC-allele 1   GCCTGTCCTGCTTTCATCAGGTGGCTGGAAGAGTTCACCTCCCAGTACTTCCAGGGATCAG    +1bp
KOC-allele 2   GCCTGTCCTGCTTTCATCAGGTGGCTGGAAGAGTTCACCTCCCAGTACCTCCAGGGATCAG    +1bp

Reference 2    TGCTTCATGAACTCCCTGCTACAAGGCCTGTCTGCCTGTCCTGCTTTCATCAGGTGGCTG TSS +228
KO11-allele 1  TGCTTCATGAACTCCCTGCTACAAGGCCTGTC--------CTGCTTTCATCAGGTGGCTG     -8bp
KO11-allele 2  TGCTTCATGAACTCCCTGCTACAAGGCCTGTCTTGCCTGTCCTGCTTTCATCAGGTGGCTG    +1bp
```

Figure S1

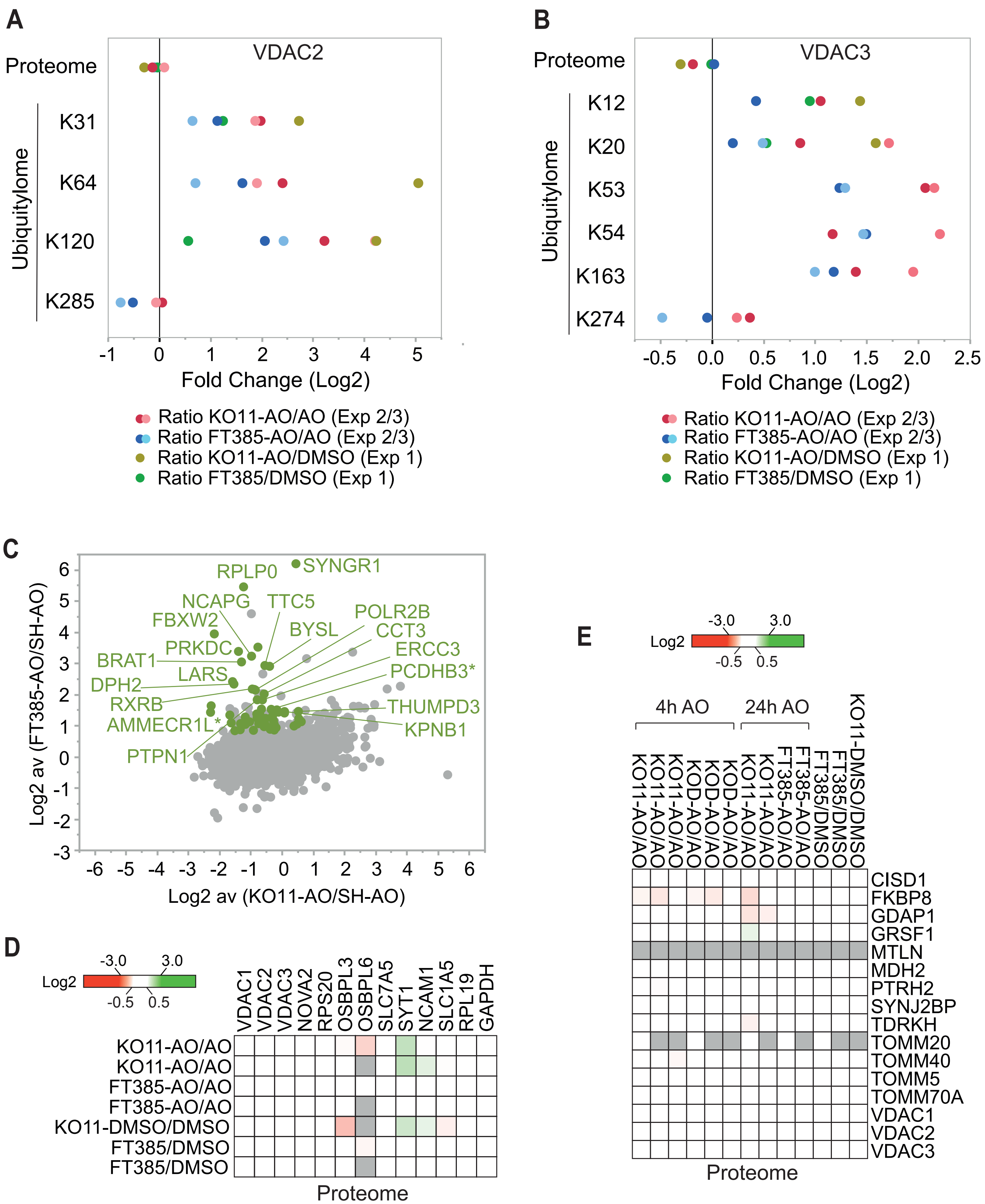

A
VDAC2
Proteome
Ubiquitylome
K31
K64
K120
K285
Fold Change (Log2)
Ratio KO11-AO/AO (Exp 2/3)
Ratio FT385-AO/AO (Exp 2/3)
Ratio KO11-AO/DMSO (Exp 1)
Ratio FT385/DMSO (Exp 1)
B
VDAC3
Proteome
Ubiquitylome
K12
K20
K53
K54
K163
K274
Fold Change (Log2)
Ratio KO11-AO/AO (Exp 2/3)
Ratio FT385-AO/AO (Exp 2/3)
Ratio KO11-AO/DMSO (Exp 1)
Ratio FT385/DMSO (Exp 1)
C
SYNGR1
RPLP0
NCAPG
TTC5
FBXW2
POLR2B
BYSL
CCT3
PRKDC
ERCC3
BRAT1
LARS
PCDHB3*
DPH2
RXRB
THUMPD3
AMMECR1L*
KPNB1
PTPN1
Log2 av (FT385-AO/SH-AO)
Log2 av (KO11-AO/SH-AO)
D
Log2
-3.0
3.0
-0.5
0.5
VDAC1
VDAC2
VDAC3
NOVA2
RPS20
OSBPL3
OSBPL6
SLC7A5
SYT1
NCAM1
SLC1A5
RPL19
GAPDH
KO11-AO/AO
KO11-AO/AO
FT385-AO/AO
FT385-AO/AO
KO11-DMSO/DMSO
FT385/DMSO
FT385/DMSO
Proteome
E
Log2
-3.0
3.0
-0.5
0.5
4h AO
24h AO
KO11-AO/AO
KO11-AO/AO
KO11-AO/AO
KOD-AO/AO
KOD-AO/AO
KOD-AO/AO
KO11-AO/AO
KO11-AO/AO
FT385-AO/AO
FT385-AO/AO
FT385/DMSO
FT385/DMSO
KO11-DMSO/DMSO
CISD1
FKBP8
GDAP1
GRSF1
MTLN
MDH2
PTRH2
SYNJ2BP
TDRKH
TOMM20
TOMM40
TOMM5
TOMM70A
VDAC1
VDAC2
VDAC3
Proteome

Figure S3

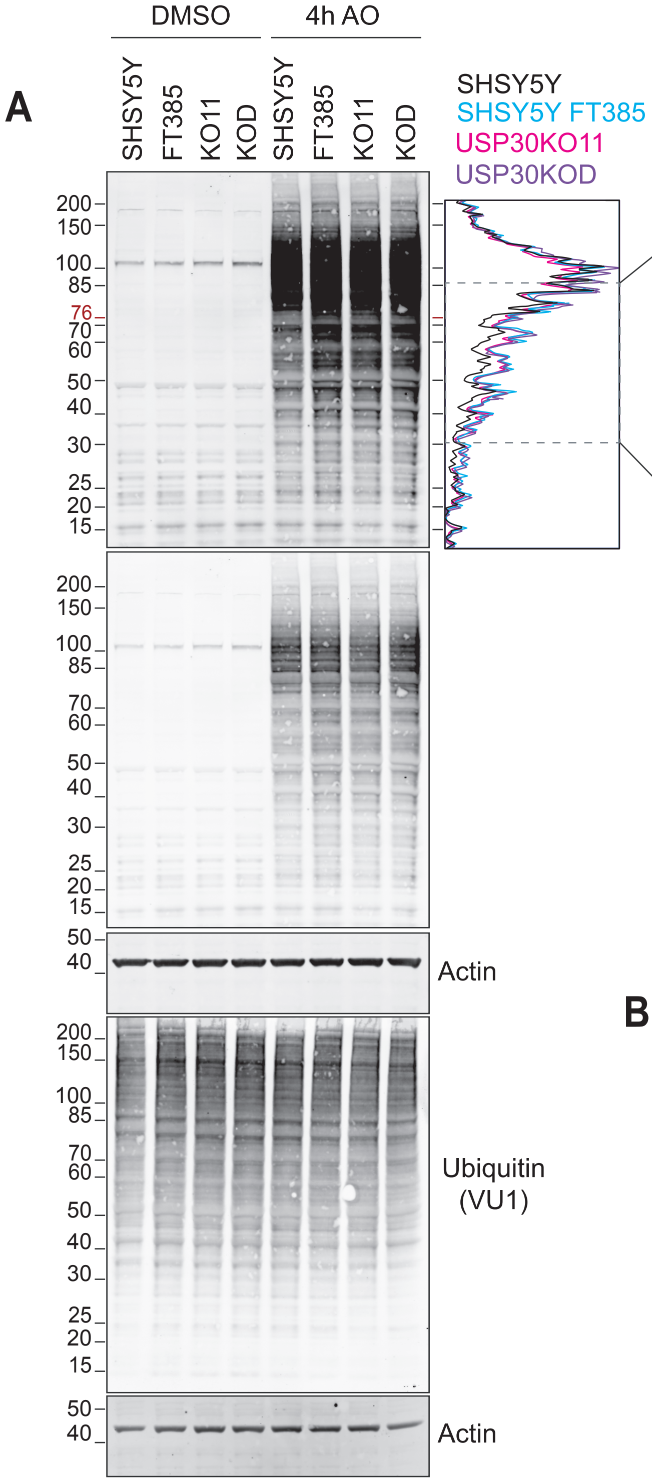
A
DMSO
4h AO
SHSY5Y
FT385
KO11
KOD
SHSY5Y
FT385
KO11
KOD
SHSY5Y
SHSY5Y FT385
USP30KO11
USP30KOD
pUb
200
150
100
85
76
70
60
50
40
30
25
20
15
Actin
Ubiquitin (VU1)

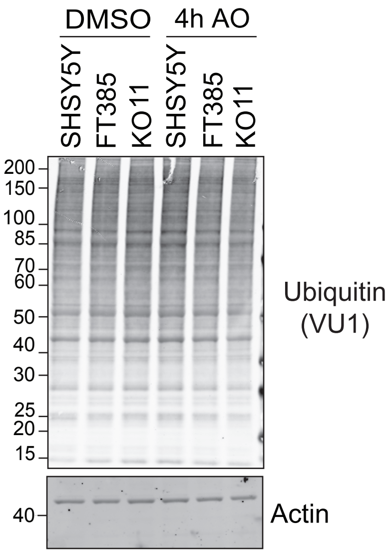
B
DMSO
4h AO
SHSY5Y
FT385
KO11
SHSY5Y
FT385
KO11
Ubiquitin (VU1)
Actin

Figure S4